

Genotypic Complexity in Initial Cleavage Divisions of Mammalian Embryos is Contributed by Defective BUB1B/BUBR1 Signaling

Kelsey E. Brooks¹, Brittany L. Daughtry^{1,2}, Brett Davis^{3,4}, Melissa Y. Yan³, Suzanne S. Fei³, Lucia Carbone⁴⁻⁷, and Shawn L. Chavez^{1,7-9*}

¹Division of Reproductive & Developmental Sciences, Oregon National Primate Research Center, Beaverton, Oregon 97006, USA

²Department of Cell, Developmental & Cancer Biology, Oregon Health & Science University, Portland, Oregon 97239, USA

³Bioinformatics & Biostatistics Unit, Oregon National Primate Research Center, Beaverton, Oregon 97006, USA

⁴Department of Medicine, Knight Cardiovascular Institute, Oregon Health & Science University, Portland, Oregon 97239, USA

⁵Division of Genetics, Oregon National Primate Research Center, Beaverton, Oregon 97006, USA

⁶Department of Medical Informatics and Clinical Epidemiology, Division of Bioinformatics & Computational Biomedicine, Oregon Health & Science University, Portland, Oregon 97239, USA

⁷Department of Molecular and Medical Genetics, Oregon Health & Science University, Portland, Oregon 97239, USA

⁸Department of Obstetrics & Gynecology, Oregon Health & Science University, Portland, Oregon 97239, USA

⁹Department of Biomedical Engineering, Oregon Health & Science University, Portland, Oregon 97239, USA

*Corresponding Author:

Shawn L. Chavez, Ph.D.
505 NW 185th Avenue
Beaverton, OR 97006
email: chavesh@ohsu.edu
phone: 503-346-5423
fax: 503-690-5563

ABSTRACT

Embryonic aneuploidy is highly complex, often leading to developmental arrest, implantation failure, and/or spontaneous miscarriage in both natural and assisted reproduction. Despite our knowledge of mitotic missegregation in somatic cells, the molecular pathways regulating chromosome fidelity during the error-prone cleavage-stage of mammalian preimplantation development remain largely undefined. Using bovine embryos and live-cell fluorescent imaging, we observed frequent micro-/multi-nucleation of missegregated chromosomes in initial divisions that persisted, re-fused with the primary nucleus, or formed a chromatin bridge with neighboring cells. A correlation between a lack of syngamy, multipolar cytokinesis, and uniparental genome segregation was also revealed and single-cell DNA-seq showed complex genotypes propagated by subsequent divisions. Depletion of the checkpoint protein, BUB1B/BUBR1, resulted in atypical cytokinesis, micro-/multi-nuclei formation, chaotic aneuploidy, and developmental arrest. This demonstrates that embryonic micronuclei sustain multiple fates, provides an explanation for blastomeres with uniparental origins, and substantiates defective BUB1B/BUBR1 signaling as a major contributor to mitotic aneuploidy.

INTRODUCTION

Multiple studies across higher-order mammalian species, including humans, have established that *in vitro*-derived embryos suffer from remarkably frequent whole chromosomal losses and gains termed aneuploidy (Chavez et al., 2012; Chow et al., 2014; Daughtry et al., 2019; J. Huang et al., 2014; Johnson et al., 2010; Vanneste et al., 2009). Depending on the type and severity of the chromosome segregation error, many aneuploid embryos will undergo developmental arrest and/or result in early pregnancy loss if transferred. Estimates of embryonic aneuploidy *in vivo* are difficult to ascertain (Miller et al., 1980; Wilcox, Weinberg, & Baird, 1995; Zinaman, Clegg, Brown, O'Connor, & Selevan, 1996), but ~50-70% of spontaneous miscarriages following natural conception in women are diagnosed as karyotypically abnormal (Hassold et al., 1980; Menasha, Levy, Hirschhorn, & Kardon, 2005; Schaeffer et al., 2004). Aneuploidy can arise either meiotically during gametogenesis, or post-zygotically from the mitotic cleavage divisions of preimplantation development. Although significant effort has been put forth to identify specific contributors to meiotic chromosome missegregation, particularly with advanced maternal age (McCoy, 2017; Schneider & Ellenberg, 2019; Webster & Schuh, 2017), much less is known about the molecular mechanisms underlying mitotic aneuploidy generation. This is in spite of findings that mitotic errors are equally or more prevalent than meiotic errors and arise independently of maternal age or fertility status (Chavez et al., 2012; Chow et al., 2014; McCoy, Demko, Ryan, Banjevic, Hill, Sigurjonsson, Rabinowitz, Fraser, et al., 2015; McCoy, Demko, Ryan, Banjevic, Hill, Sigurjonsson, Rabinowitz, & Petrov, 2015; Vanneste et al., 2009). Since the first three mitotic divisions are the most error-prone and activation of the embryonic genome does not occur until the 4- to 8-cell stage in the majority of mammals (Braude, Bolton, & Moore, 1988; Dobson et al., 2004; Plante, Plante, Shepherd, & King, 1994), it was suggested that maternally-inherited signaling factors regulating early mitotic chromosome segregation may be lacking or compromised in mammalian preimplantation embryos (Mantikou, Wong, Repping, & Mastenbroek, 2012; Taylor et al., 2014; Tsuiiko et al., 2019).

There are several known contributors to aneuploidy and tumorigenesis in somatic cells, such as loss or prolonged chromosome cohesion, defective spindle attachments, abnormal centrosome number, and

relaxed cell cycle checkpoints (Ganem, Godinho, & Pellman, 2009; Soto, Raaijmakers, & Medema, 2019). Regardless of the mechanism, chromosomes that are missegregated during meiosis or mitosis will become encapsulated into micronuclei and can contribute to aneuploidy in subsequent divisions. In embryos, research has primarily focused on the spindle assembly checkpoint (SAC) and mostly with mice that normally exhibit a low incidence of micronucleation and aneuploidy (Lightfoot, Kouznetsova, Mahdy, Wilbertz, & Hoog, 2006; Macaulay et al., 2015; Treff et al., 2016; Vazquez-Diez, Yamagata, Trivedi, Haverfield, & FitzHarris, 2016). Thus, murine embryos are often treated with chemicals that inhibit spindle formation or SAC function to induce chromosome missegregation (Bolton et al., 2016; Singla, Iwamoto-Stohl, Zhu, & Zernicka-Goetz, 2020; Vazquez-Diez, Paim, & FitzHarris, 2019b; Wei et al., 2011), which target multiple genes and can have variable or off-target effects (S. Chen et al., 2007; Gascoigne & Taylor, 2008; Miyazawa, 2011). By monitoring bipolar attachment of spindle microtubules to kinetochores during mitosis, the mitotic checkpoint complex (MCC) prevents activation of the anaphase promoting complex/cyclosome (APC/C) and delays mitotic progression in the absence of stable bipolar kinetochore-microtubule attachments (Fogarty et al., 2017). This delay, however, is only temporary and cells with an unsatisfied checkpoint will eventually arrest or exit mitosis prematurely. The core components of the MCC are evolutionarily conserved and include CDC20, as well as the serine/threonine kinases, BUB1B, BUB3, and MAD2. BUB1B (also known as BUBR1), the largest of the MCC proteins, is normally present throughout the cell cycle and proposed to have both SAC-dependent and independent functions (Elowe et al., 2010). Besides being directly associated with unattached or incorrectly attached kinetochores, BUB1B also has a role in stabilizing kinetochore-microtubule attachments and chromosome alignment via BUB3 binding (Meraldi & Sorger, 2005; G. Zhang, Mendez, Sedgwick, & Nilsson, 2016). Without BUB1B, the MCC no longer localizes to unattached kinetochores to prevent incorrect or deficient spindle attachments, resulting in the generation of aneuploid daughter cells (Homer, Gui, & Carroll, 2009; Lampson & Kapoor, 2005). Whether the MCC is functional in the initial mitotic divisions of mammalian embryogenesis is currently unclear (Vazquez-Diez et al., 2019b; Wei et al., 2011) and remains to be studied in a mammal that undergoes a high incidence of mitotic aneuploidy in the absence of chemical induction.

Cattle typically ovulate only one mature oocyte-containing follicle per month and share other key characteristics of preimplantation development with humans, including the timing of the first mitotic divisions, stage at which the major wave of embryonic genome activation (EGA) occurs, and approximate percentage of embryos that typically reach the blastocyst stage (Alper, Brinsden, Fischer, & Wikland, 2001; Sugimura et al., 2012; Wong et al., 2010). Furthermore, single-nucleotide polymorphism (SNP) genotyping and next generation sequencing (NGS) revealed that the frequency of aneuploidy (~32-85%) in cattle is likely similar to humans (Destouni et al., 2016; Hornak et al., 2016; Tsuiko et al., 2017). Destouni *et al.* also demonstrated that bovine zygotes can segregate parental genomes into different blastomeres during the first cleavage division, but the mechanism by which this occurs has not yet been determined (Destouni et al., 2016). Thus, with the ethical and technical limitations of human embryo research, bovine embryos represent a suitable model for studying the dynamics of micronuclei formation and aneuploidy generation during preimplantation development. In this study, we used a combination of time-lapse and live-cell fluorescent imaging with single-cell DNA-seq (scDNA-seq) for copy number variation (CNV) analysis, to assess mitotic divisions in bovine embryos from the zygote to 12-cell stage and visualize chromosome segregation in real-time. We also evaluated the lack of MCC function on cytokinesis, micronucleation, mitotic aneuploidy, and developmental arrest, characteristics commonly observed during early embryogenesis in higher-order mammals.

RESULTS

Micronuclei formation is relatively common in early cleavage-stage bovine embryos

Although micronuclei-like structures have been detected in bovine embryos previously (Yao et al., 2018), their prevalence or whether they were associated with a particular stage of preimplantation development was not determined. To address this, we generated a large number (N=53) of bovine embryos by *in vitro* fertilization (IVF) and fixed them at the zygote to blastocyst stage to evaluate DNA integrity with DAPI and nuclear structure by immunostaining for the nuclear envelope marker, LAMIN-B1 (LMNB1; **Fig. 1A**). Immunofluorescent labeling revealed the presence of micronuclei as early as the zygote stage that were distinct from the maternal and paternal pronuclei (**Fig. 1B**). Several micronuclei, as well as multiple nuclei (multinuclei) of similar size, were also detected at the 2- to 4-cell stage (**Fig. 1C**). Overall, ~37.7% (N=20/53) of early cleavage-stage bovine embryos exhibited micro-/multi-nuclei formation in one or more blastomeres. This suggests that unlike mice, which rarely exhibit micronucleation during initial mitotic divisions (Vazquez-Diez et al., 2019b), encapsulation of missegregated chromosomes into micronuclei prior to EGA is conserved between cattle and primates (Chavez et al., 2012; Daughtry et al., 2019). A similar examination of bovine blastocysts also immunostained for the trophoblast marker, Caudal Type Homeobox 2 (CDX2), demonstrated that micronuclei often reside in the trophectoderm (TE; **Fig. 1D**), but can also be contained within the inner cell mass (ICM) of the embryo (**Fig. 1E**).

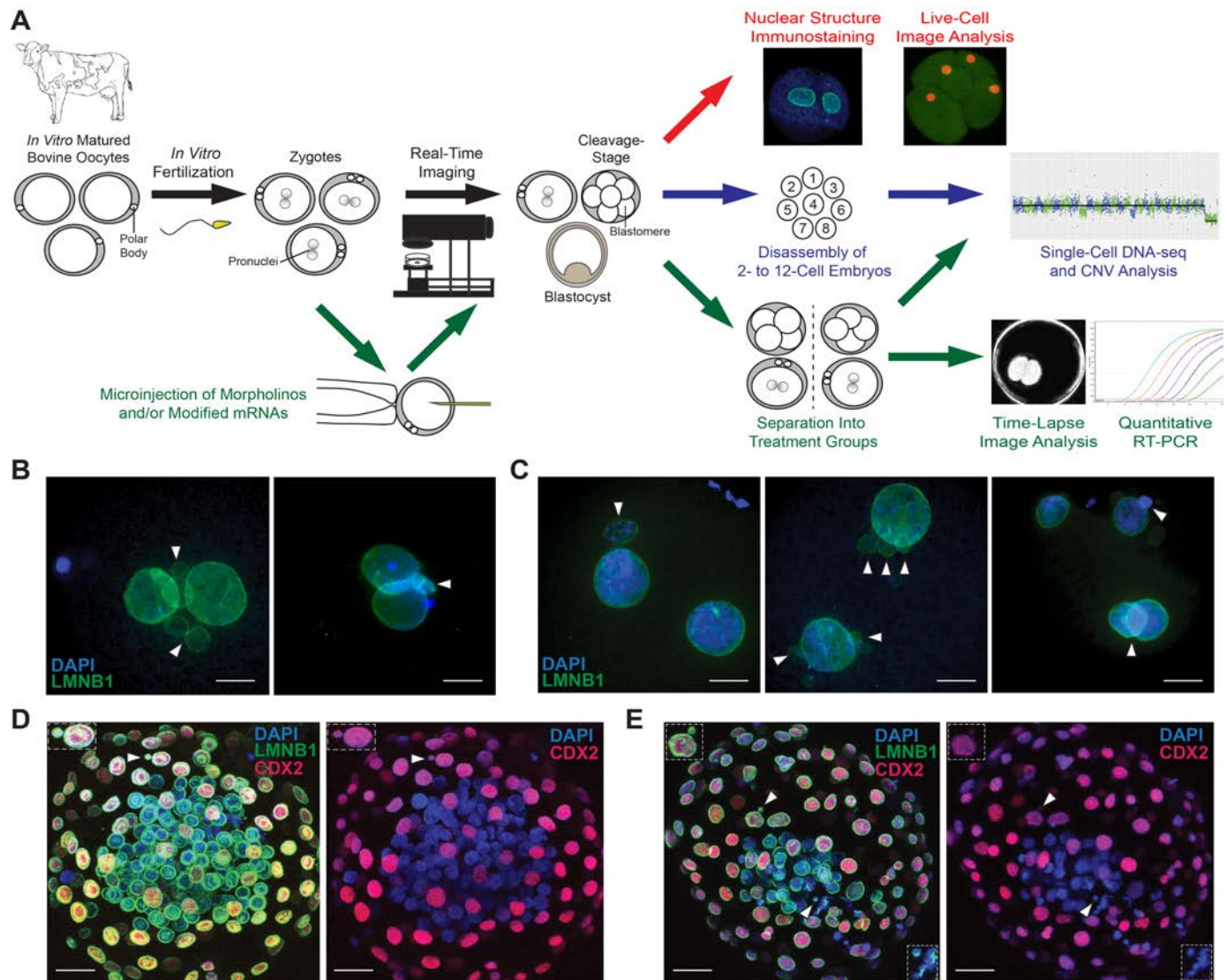


Figure 1: Investigating the dynamics of mitotic chromosome segregation and MCC fidelity in bovine embryos. (A) *In vitro* produced bovine oocytes underwent IVF and the resulting zygotes non-invasively monitored by time-lapse image analysis until collection for immunostaining of nuclear structure. Another subset of zygotes was microinjected with fluorescently labeled modified mRNAs and chromosome segregation visualized during the first three mitotic divisions in real-time by live-cell confocal microscopy. Cleavage-stage embryos were disassembled into single blastomeres at the 2- to 12-cell stage for scDNA-seq and CNV analysis to determine the precise frequency of aneuploidy at multiple cleavage stages. Other zygotes were microinjected with non-overlapping morpholinos targeting the mitotic checkpoint protein, BUB1B, and/or modified BUB1B mRNA to test the effect and specificity of BUB1B inhibition on chromosome segregation, division dynamics, and preimplantation development. Gene expression profiling was also conducted on a subset of BUB1B deficit zygotes versus controls by quantitative RT-PCR to identify changes in gene abundance and molecular pathways associated with BUB1B knockdown. (B) Immunostaining of zygotes and (C) cleavage-stage embryos with LMNB1 (green) using DAPI (blue) to visualize DNA revealed several micro- and multi-nuclei (white arrows). (D) Blastocysts also immunostained for the trophoblast marker, CDX2 (red), showed that micronuclei are often present in the TE, (E) but can also be retained within the ICM of the embryo. Scale bar = 10 μ m.

Live-cell fluorescent imaging reveals micronuclei fate and the origin of uniparental cells

To confirm the frequency of micro- and multi-nuclei in cleavage-stage embryos and determine the fate of these nuclear structures in real-time, we microinjected bovine zygotes (N=90) with fluorescently labeled modified mRNAs and monitored the first three mitotic divisions by live-cell confocal microscopy (**Fig. 1A**). While Histone H2B and/or LMNB1 were used to visualize DNA and nuclear envelope, respectively, F-actin was injected to distinguish blastomeres (**Supplemental Movie S1**). Of the microinjected embryos, ~18.9% (N=17/90) failed to complete cytokinesis during microscopic evaluation, while ~53.3% (N=49/90) exhibited normal bipolar divisions and ~27.8% (N=25/90) underwent multipolar divisions from 1- to 3-cells or more (**Fig. 2A**). In accordance with our immunostaining findings, ~31.1% (N=28/90) of the embryos contained micro- and/or multi-nuclei and anaphase lagging of chromosomes was detected prior to their formation in three of these embryos at the zygote (**Fig. 2B**) or 2-cell stage (**Fig. 2C**). Micro- and multi-nucleation was more frequently associated with bi-polar divisions (**Fig. 2A**) and an examination of micronuclei fate demonstrated an equal incidence of unilateral inheritance (**Fig. 2D**) or fusion back with the primary nucleus (**Fig. 2E**), while a smaller percentage appeared to form a chromatin bridge between blastomeres (**Fig. 2F**, **Supplemental Fig. S2** and **Supplemental Movie S1**). Interestingly, the majority of multipolar embryos (76%; N=19/25) underwent the abnormal division after bypassing syngamy, or the fusion of maternal and paternal pronuclei (**Fig. 2G**), and/or produced daughter cells that did not contain any apparent nuclear structure (**Fig. 2H**). These results helped explain previous findings of blastomeres with uniparental origins and those that completely lacked nuclear DNA when assessed by SNP genotyping and/or NGS (Daughtry et al., 2019; Destouni et al., 2016; Middelkamp et al., 2020).

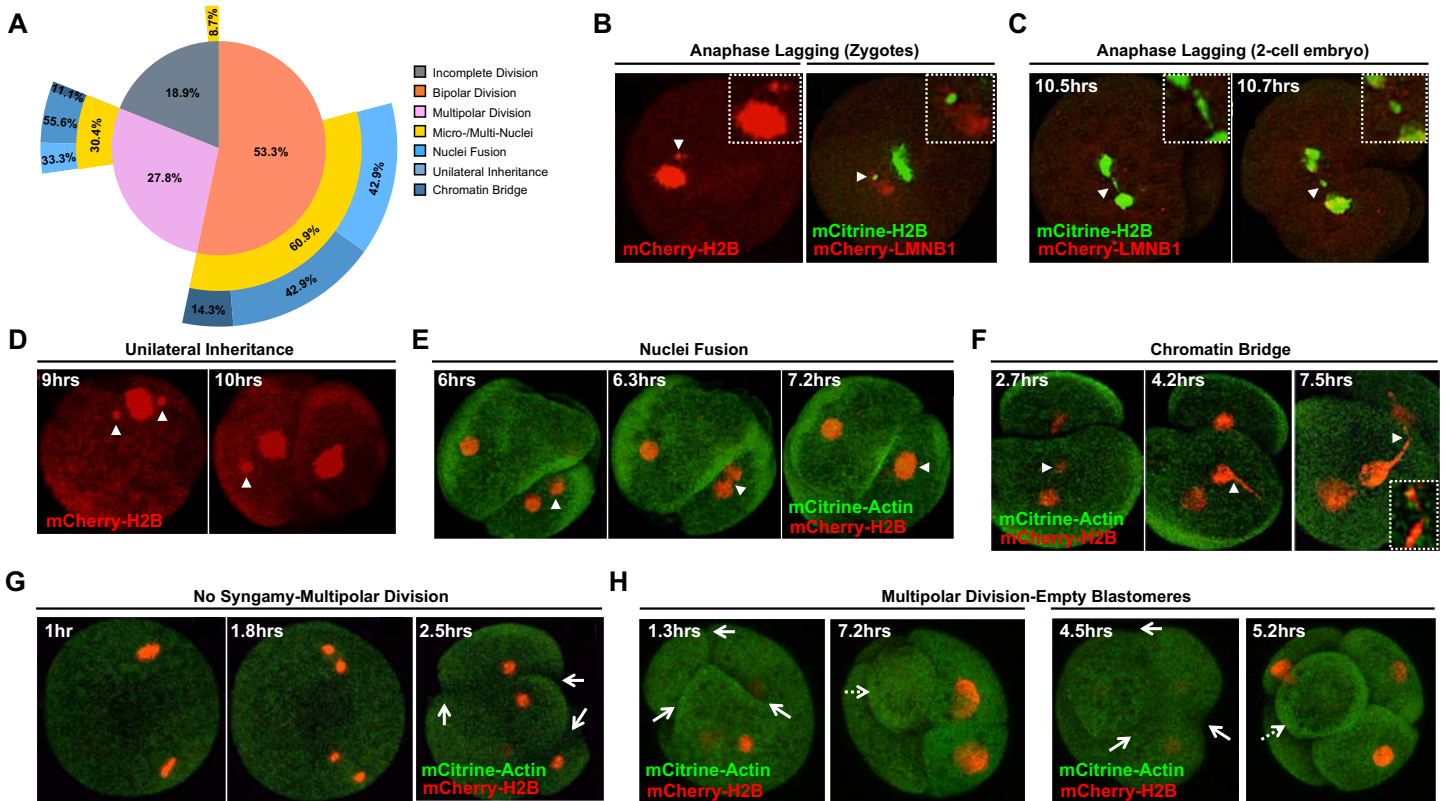


Figure 2: Live-cell fluorescent imaging reveals micronuclei fate and uniparental genome distribution to daughter cells. Bovine zygotes were microinjected with fluorescently labeled modified mRNAs (mCitrine or mCherry) to visualize DNA (Histone H2B) or nuclear structure (LMNB1) and distinguish blastomeres (F-Actin) by live-cell confocal microscopy during the first three mitotic divisions. **(A)** A Venn-Pie that shows the percentage of embryos that did not complete cytokinesis (gray), exhibited normal bipolar divisions (orange), or underwent multipolar divisions at the zygote or 2-cell stage (pink). The percentage of embryos with micro- and/or multi-nuclei (MN; yellow) associated with each type of division is also shown. Micronuclei fate is represented as those that formed a chromatin bridge (dark blue), exhibited unilateral inheritance (medium blue), or re-fused with the primary nucleus (light blue). Note that most embryos underwent bipolar divisions and were more likely to contain micronuclei than multipolar embryos. **(B)** Anaphase lagging of chromosomes (white arrowheads) was detected in certain embryos at the zygote or **(C)** 2-cell stage prior to micronuclei formation. **(D)** An examination of micronuclei fate demonstrated that a relatively equal proportion persist and undergo unilateral inheritance or **(E)** fuse back with the primary nucleus, **(F)** with a small number exhibiting what appeared to be a chromatin bridge between blastomeres following micronuclei formation (white arrowheads). **(G)** The majority of multipolar embryos (white solid arrows) bypassed pronuclear fusion (syngamy) prior to the abnormal division and **(H)** often produced blastomeres with uniparental origins and/or no apparent nuclear structure (white dashed arrows). Numbers in upper left corner represent the time in hours (hrs) since the start of imaging.

Non-reciprocal mitotic errors and chaotic aneuploidy are propagated by subsequent divisions

Although SNP arrays or NGS have been used previously to assess aneuploidy in cleavage-stage bovine embryos, these studies were limited as they reported a large range in aneuploidy frequency (~32-85%), examined a single stage of development, and/or evaluated only a portion of the embryo (Destouni et al., 2016; Hornak et al., 2016; Tsuiko et al., 2017). Therefore, our next objective was to determine the precise frequency of aneuploidy in a large number of bovine embryos (N=38) disassembled into individual cells at multiple cleavage stages (**Fig. 1A** and **Supplemental Table 1**). All cells from the 38 embryos were assessed to ensure an accurate representation of the overall embryo, resulting in a total of 133 blastomeres analyzed from the 2- to 12-cell stage (**Fig. 3A**). Based on previously described criteria (Daughtry et al., 2019), we classified 25.6% (N=34/133) of blastomeres as euploid, 35.3% (N=47/133) as aneuploid, 3% (N=4/133) solely containing segmental errors, and 17.3% (N=23/133) exhibiting chaotic aneuploidy, with the remaining cells either failing WGA (10.5%; N=14/133) or identified as empty due to the amplification and detection of only mitochondrial DNA (8.3%; N=11/133). After reconstructing each embryo, we determined that ~16% (N=6/38) were entirely euploid, whereas ~55% (N=21/38) were comprised of only aneuploid cells (**Fig. 3B**). An additional ~29% (N=11/38) were categorized as mosaic since they contained a combination of both euploid and aneuploid blastomeres, of which ~18% (N=2/11) had incurred segmental errors only, or DNA breaks of 15 Mb in length or larger that did not affect the whole chromosome. The X chromosome was by far the most frequently impacted by whole chromosomal losses and gains, whereas chromosome 5 (human chromosomes 12 and 22), 7 (human chromosomes 5 and 19), 11 (human chromosomes 3 and 9), and 29 (human chromosome 11) were commonly subjected to DNA breakage (**Fig. 3C**). While meiotic missegregation was identified in ~16% (N=6/38) of the embryos (**Fig. 3D**), mitotic aneuploidy accounted for the majority (~66%; N=25/38) of errors, with the remaining ~18% (N=7/38) exhibiting the genotypic complexity characteristic of chaotic aneuploidy (**Fig. 3E**). Of the embryos with meiotic errors, many (~67%; N=4/6) also experienced mitotic missegregation of different chromosomes than those originally affected during meiosis (**Fig. 3F**). Moreover, reciprocal

losses and gains, whereby chromosomes lost from one blastomere were found in a sister blastomere, accounted for only ~25% (N=8/29) of the mitotic errors (Fig. 3D and 3F).

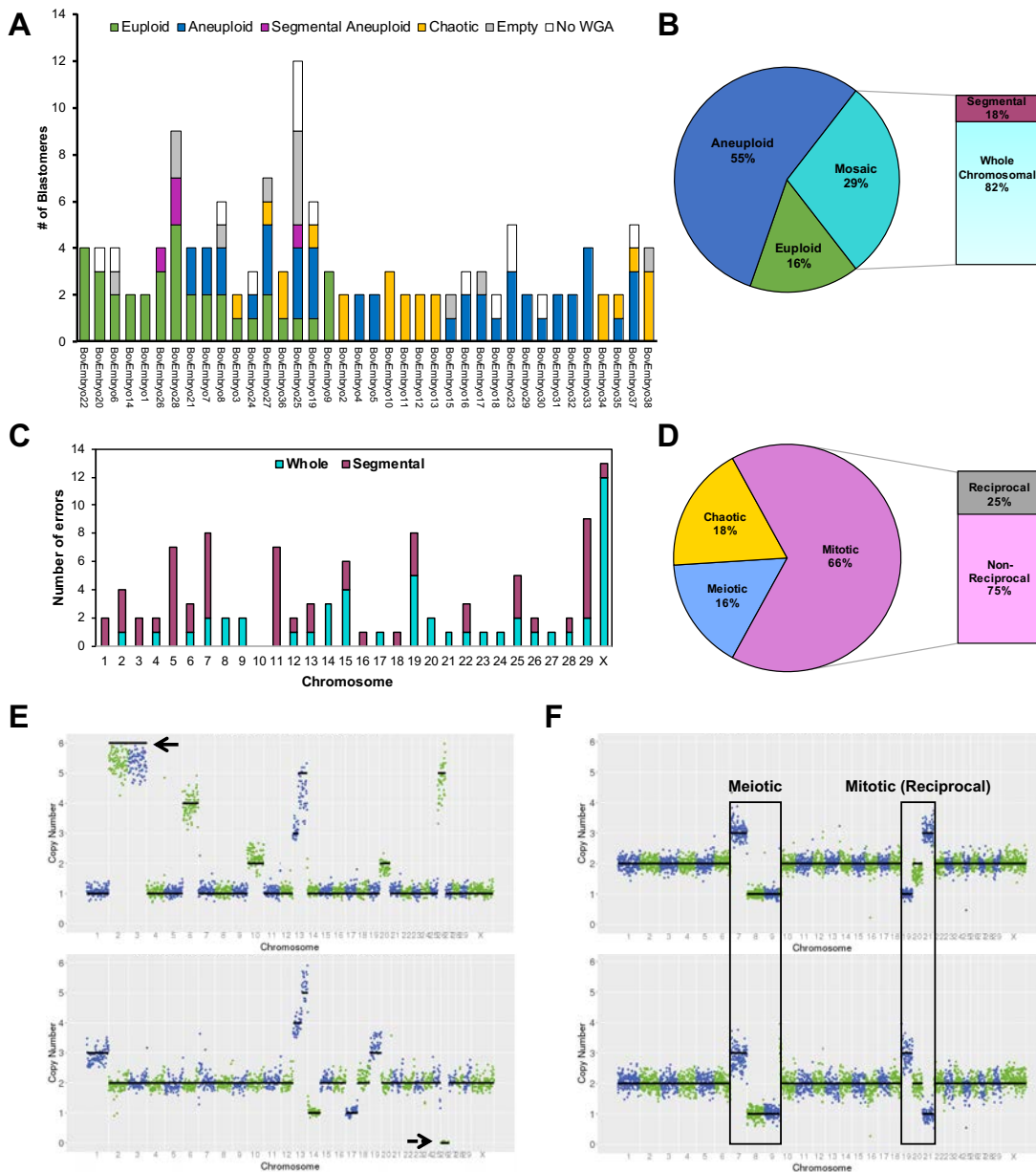


Figure 3: Comprehensive assessment of chromosomal abnormalities in early cleavage-stage embryos by scDNA-seq. (A) Whole chromosome and sub-chromosomal CNV was evaluated in bovine embryos from the 2- to 12-cell stage (N=38). Stacked bars represent all blastomeres (N=133) classified as euploid (green), aneuploid (blue), segmental aneuploid (purple), chaotic aneuploid (yellow), empty (grey) or failing to undergo WGA (white). **(B)** Pie chart showing the overall chromosomal status of the embryos. **(C)** Number of whole or segmental chromosome losses and/or gains affecting each chromosome. Note the frequent missegregation of the X-chromosome and DNA breakage in chromosomes 5, 7, 11, and 29. **(D)** The percentage of aneuploid embryos with each type of chromosomal error. **(E)** CNV plots of blastomeres from two different embryos with chaotic aneuploidy showing up to 6 copies of certain chromosomes (top; black solid arrow) and a complete loss of other chromosomes (bottom; black dashed arrow). **(F)** Blastomeres from a 2-cell embryo with meiotic errors (Ch.7, 8, and 9) propagated during the first cleavage division that also experienced mitotic missegregation of different chromosomes (Ch.19 and 21) that were reciprocal.

BUB1B deficiency induces multipolar divisions, blastomere asymmetry and mitotic arrest

Since the chromosome constitution and division dynamics observed in certain bovine embryos suggested a lack of adequate cell cycle checkpoints, our next objective was to determine whether the loss of MCC function was associated with micronuclei formation and aneuploidy at the early cleavage stage (**Fig. 1A**). We focused our attention on BUB1B, the largest of the MCC proteins present throughout the cell cycle that helps ensure that inhibition of anaphase until the kinetochores of all chromosomes are correctly attached to the mitotic spindle (Elowe et al., 2010). Two non-overlapping morpholino antisense oligonucleotides (MAOs) were designed to specifically inhibit the translation of BUB1B mRNA by targeting the ATG translation start site (BUB1B MAO #1) or a sequence upstream within the 5' UTR (BUB1B MAO #2) and tested before use in embryos (**Supplemental Fig. S2**). Bovine zygotes were microinjected with either BUB1B MAO #1 (N=48), BUB1B MAO #2 (N=36), or Std Control MAO (N=81) and cultured under a time-lapse imaging microscope to monitor developmental dynamics. Each embryo was morphologically assessed and categorized as having either normal or abnormal divisions for comparison to untreated (non-injected) embryos (N=180). In the BUB1B MAO #1 treatment group, a large percentage (37.5%; N=18/48) of the zygotes failed to undergo the first cleavage division (**Table 1**) and a subset (8.3%; N=4/48) of these embryos attempted to divide by forming cleavage furrows multiple times (**Fig. 4A**), but never successfully completed cytokinesis (**Supplemental Movie S2**). Of those BUB1B MAO #1 zygotes that did divide, only a small proportion (18.8%; N=9/48) were normal bipolar divisions. Instead, many embryos (63.0%; N=17/27) exhibited abnormal cleavage, including multipolar divisions and/or blastomere asymmetry (**Supplemental Movie S3** and **Supplemental Movie S4**, respectively), with similar results obtained following injection with the BUB1B MAO #2 (**Table 1** and **Fig. 4B**). Despite the phenotypic similarities between the two non-overlapping MAOs, we further assessed BUB1B MAO specificity by conducting embryo rescue experiments with modified BUB1B mRNA that would not be directly targeted by the MAO. BUB1B mRNA with a mutated MAO binding sequence was microinjected into bovine zygotes, along with BUB1B MAO #1 (N=85), and embryos cultured up to the blastocyst stage (**Fig. 4C**). While no embryos formed blastocysts following injection of either the BUB1B MAO #1 or #2, 45% (N=23/51) of the BUB1B MAO #1+mRNA co-injected embryos underwent cleavage

divisions and reached the blastocyst stage (**Fig. 4D**). This percentage was similar to that obtained from the non-injected embryos and following injection with the Std Control MAO, confirming that the knockdown of BUB1B expression and rescue of BUB1B-induced mitotic defects were specific.

	Untreated (Non-Injected)	Std Control MAO	BUB1B MAO #1	BUB1B MAO #2
No Division	8.3% (N=15/180)	24.7% (N=20/81)	37.5% (N=18/48)	33.3% (N=12/36)
Attempted Division	10% (N=18/180)	2.5% (N=2/81)	8.3% (N=4/48)	0.0% (N=0/36)
Normal Bipolar/ Symmetric Division	72.8% (N=107/147)	62.7% (N=37/59)	34.6% (N=9/26)	25.0% (N=6/24)
Abnormal Multipolar/ Asymmetric Division	27.2% (N=40/147)	37.3% (N=22/59)	65.4% (N=17/26)	75.0% (N=18/24)
Total Number of Embryos	180	81	48	36

Table 1: Division dynamics in untreated and MAO embryo treatment groups. Summary of the percentage of bovine zygotes that exhibited no division or attempted to divide as well as those that had normal bipolar/symmetric versus abnormal multipolar/asymmetric divisions following no treatment or microinjection with Std Control, BUB1B MAO #1, or BUB1B MAO #2. Attempted division was defined by the identification of cleavage furrows without the completion of cytokinesis. Note that in contrast to the controls, BUB1B MAO #1 and BUB1B MAO #2-injected embryos were more likely to undergo multipolar and/or asymmetric divisions.

BUB1B-deficient embryos exhibit chaotic aneuploidy and asymmetric genome distribution

Because BUB1B MAO-injected embryos exhibited atypical cytokinesis and mitotic arrest, we examined nuclear structure and CNV in BUB1B-deficient embryos by immunofluorescence and scDNA-seq, respectively (**Fig. 1A**). LMNB1 immunostaining of BUB1B MAO #1 and #2 treated bovine embryos revealed both micro- and multi-nuclei in embryos that did not attempt division or were unable to complete the first cytokinesis (**Fig. 4E**). Similar abnormal nuclear structures, as well as empty blastomeres, were also observed in BUB1B MAO-injected embryos that successfully divided. Moreover, DNA that lacked or had defective nuclear envelope was apparent in the blastomeres of BUB1B deficient cleavage-stage embryos. Disassembly of the embryos into individual cells for assessment of DNA content and CNV analysis demonstrated that while some euploid blastomeres were obtained following BUB1B MAO injection, BUB1B deficiency mostly produced blastomeres with chaotic aneuploidy (**Fig. 4F**). Analogous to the uninjected controls with chaotic aneuploidy (**Fig. 3E**), a complete loss of certain chromosomes and

a gain of up to 5-6 copies of other chromosomes were detected, suggesting that the lack of BUB1B permits asymmetrical genome distribution in embryos.

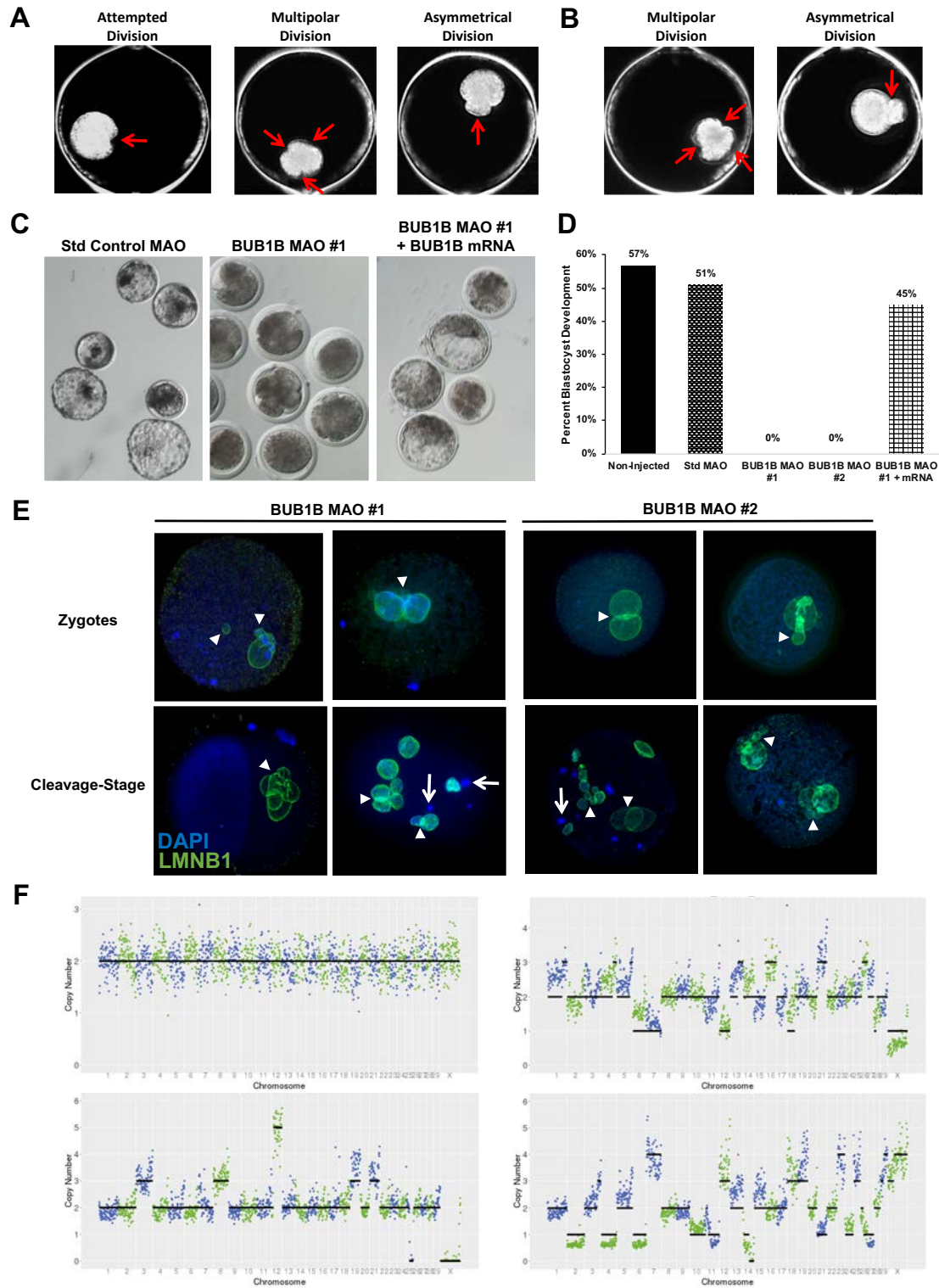


Figure 4: BUB1B knockdown induces multipolar divisions, chaotic aneuploidy, and developmental arrest. (A) Darkfield time-lapse imaging frames depicting the various embryo phenotypes (red arrows), including attempted division, multipolar division, and blastomere asymmetry observed following BUB1B MAO #1 or (B) BUB1B MAO #2 microinjection in bovine zygotes. (C) Representative stereomicroscope images of embryos and blastocysts from the Std control MAO, BUB1B MAO #1, and BUB1B MAO #1 plus BUB1B modified mRNA treatment groups. (D) Bar graph of the percentage of embryos that reached the blastocyst stage in non-injected, Std control MAO, BUB1B MAO #1, BUB1B MAO #2, or BUB1B MAO #1 plus BUB1B modified mRNA injected zygotes. While no blastocysts were obtained following BUB1B MAO #1 or #2 treatment, the co-injection of BUB1 MAO #1 and BUB1B modified mRNA was able to almost fully rescue the phenotype and restore blastocyst formation rates to that observed in controls. (E) Confocal images of LMNB1 (green) immunostaining in BUB1B MAO #1 or #2 treated embryos stained with DAPI (blue). Severely abnormal nuclear morphology and the presence of both micro- and multi-nuclei were detected (denoted with white arrowheads) in embryos at the zygote stage (top row) and cleavage-stage that exhibited abnormal cell divisions (bottom row). Note the DNA without nuclear envelope (white arrows) and the blastomere that completely lacked nuclear material in the 2-cell embryo located in the lower left image; Scale bars = 10 μ m. (E) CNV plots of blastomeres from different cleavage-stage embryos disassembled into single cells following BUB1B #1 MAO injection. While some euploid blastomeres were detected in BUB1B-injected embryos (upper left plot), most exhibited chaotic aneuploidy with multiple whole and sub-chromosomal losses and gains.

Lack of BUB1B in zygotes impacts expression of other mitosis and cell cycle-related genes

Given that inappropriate expression of maternally-inherited signaling factors has been suggested to regulate early mitotic chromosome segregation in mammalian preimplantation embryos (Mantikou et al., 2012; Taylor et al., 2014; Tsuiko et al., 2019), we next determined whether BUB1B deficiency impacted the expression of other key genes (**Fig. 1A**). Therefore, the relative abundance of mitotic, cell cycle, developmentally-regulated, and cell survival genes was assessed in individual BUB1B MAO #1 versus non-injected and Std Control-injected MAO embryos (**Supplemental Fig. S3** and **Supplemental Table 2**) via microfluidic quantitative RT-PCR (qRT-PCR). Besides *BUB1B*, other genes involved in cytokinesis and chromosome segregation such as amyloid beta precursor protein binding family B member 1 (*APBB1*), which inhibits cell cycle progression, aurora kinase B (*AURKB*), Polo-like kinase 1 (*PLK1*), and Ribosomal protein S6 kinase alpha-5 (*RPS6KA5*) were significantly downregulated in BUB1B MAO-injected embryos relative to the controls (**Fig. 5A**; $p \leq 0.05$). Additional genes, including those associated with the extracellular matrix (cartilage acidic protein 1; *CRTAC1* and ADAM metallopeptidase with thrombospondin type 1 motif 2; *ADAMTS2*) and stress response (Endoplasmic Reticulum Lectin 1; *ERLEC1*) were also significantly decreased in BUB1B deficient embryos in comparison to the non-injected and Std Control MAO-injected embryos. In contrast, genes involved in cell cycle progression

such as Epithelial Cell Transforming 2 (*ECT2*), pogo transposable element derived with ZNF domain (*POGZ*), centromere protein F (*CENPF*), and Ribosomal protein S6 kinase alpha-4 (*RPS6KA4*), were significantly upregulated in BUB1B MAO-injected embryos, along with microtubule polymerization (*HAUS* augmin like complex subunit 6; *HAUS6*) or orientation (Synaptonemal complex protein 3; *SCP3*) genes (**Fig. 5B**; $p \leq 0.05$). Thus, in the absence of BUB1B, we postulate that zygotes still entered mitosis, but were unable to obtain proper microtubule-kinetochore attachments prior to the first cytokinesis despite several attempts. This resulted in dysregulation of other genes important for mitotic exit, cytokinesis, and chromosome segregation, suggesting that inhibition of the MCC via reduced BUB1B abundance does indeed impact early cleavage divisions in higher mammals.

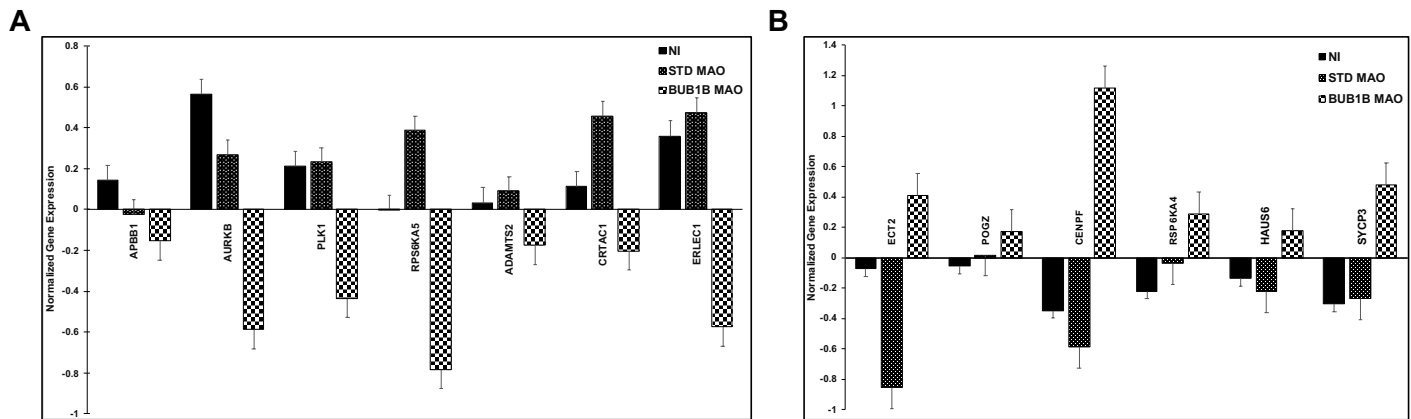


Figure 5. BUB1B deficiency in zygotes impacts the abundance of other cell cycle and mitosis-related genes. The relative abundance of several mitotic, cell cycle, developmentally-regulated, and cell survival genes was assessed via microfluidic quantitative RT-PCR (qRT-PCR) in non-injected (NI; N=5), Std Control MAO (N=5), and BUB1B MAO #1 (N=5) individual zygotes using gene-specific primers. **(A)** The genes that were significantly downregulated ($p \leq 0.05$) in BUB1B MAO-injected embryos compared to the NI and Std Control MAO groups \pm standard error is shown in the bar graph. **(B)** A bar graph of the genes that were significantly upregulated in BUB1B MAO-injected embryos relative to the controls \pm standard error. The full list of the 96 genes with primer sequences assessed by qRT-PCR is available in **Supplemental Fig. S3** and **Supplemental Table S2**, respectively.

DISCUSSION

Aneuploidy is a major cause of embryo arrest, implantation failure, and spontaneous miscarriage across most mammalian species. Yet, relatively little is still known about the molecular mechanism(s) underlying aneuploidy generation and pregnancy loss during embryonic or fetal development. Of the known factors that contribute to aneuploidy and tumorigenesis in somatic cells, only cell cycle checkpoints have been examined during embryogenesis (Bolton et al., 2016; Singla, Iwamoto-Stohl, Zhu, & Zernicka-Goetz, 2020; Vazquez-Diez, Paim, & FitzHarris, 2019b; Wei et al., 2011). Unlike tumors and cancer cells, which often overexpress SAC proteins and rarely sustain SAC gene mutations (Schvartzman, Sotillo, & Benezra, 2010), cleavage-stage human embryos tend to underexpress cell cycle checkpoints (Kieśliling et al., 2009, 2010). Knockout or hypomorphic studies of the core SAC component, BUB1B/BUBR1, was shown to result in meiotic missegregation, postimplantation lethality, infertility, and aging (Baker et al., 2004; Schmid et al., 2014; Touati et al., 2015). Relatively few studies, however, have investigated the role of specific SAC proteins in early cleavage divisions when mitotic aneuploidy typically occurs (Vazquez-Diez, Paim, & FitzHarris, 2019a). Additionally, these studies were conducted in mouse embryos, which naturally exhibit a low incidence (~1-4%) of aneuploidy (Lightfoot et al., 2006; Macaulay et al., 2015; Treff et al., 2016) unless chemically induced (Bolton et al., 2016; Singla et al., 2020; Vazquez-Diez et al., 2019b; Wei et al., 2011). Using a combination of live-cell imaging and single-cell DNA-seq, here we visualized mitotic chromosome segregation in real-time from the zygote to the ~12-cell stage and assessed the specific role of BUB1B in embryos from a monovulatory animal model that suffers from a comparable incidence of aneuploidy and developmental arrest as humans.

While micronuclei-like structures have been previously detected in bovine embryos (Yao et al., 2018), we were able to assess their prevalence throughout preimplantation development and follow their fate in subsequent mitotic divisions. Of the cleavage-stage bovine embryos examined by immunostaining or live-cell imaging, over ~30% contained micro- or multi-nuclei and anaphase lagging of chromosomes was detected in certain embryos prior to micronuclei formation. When we evaluated other cellular behaviors that might indicate how these atypical nuclear structures formed, we observed that most micronuclei-

containing embryos underwent normal bipolar divisions, excluding abnormal cytokinesis as the primary mechanism. However, multipolar divisions were associated with a lack of syngamy and often produced cells that did not contain any apparent nuclear structure (**Fig. 6A**). Unlike mouse embryos, which exhibit spatial separation of parental genomes by dual-spindle formation (Mayer, Smith, Fundele, & Haaf, 2000; Reichmann et al., 2018), bovine embryos normally undergo syngamy at the zygote stage (Yao et al., 2018). By avoiding syngamy and undergoing multipolar cytokinesis, zygotes differentially segregate entire parental genomes to daughter cells, helping to explain previous findings of heterogoneic divisions and the production of blastomeres with uniparental origins in both cattle and primates (Daughtry et al., 2019; Destouni et al., 2016; Middelkamp et al., 2020). Examination of micronuclei fate in subsequent divisions revealed an equal incidence of unilateral inheritance and fusion back with the primary nucleus, with a smaller percentage of embryos exhibiting a chromatin bridge between blastomeres following micronuclei formation (**Fig. 6B**). Because cancer cell micronuclei have been shown to contain extensive DNA damage upon re-fusion with the primary nucleus (Crasta et al., 2012; Y. Huang et al., 2012; C. Z. Zhang et al., 2015), whether there are differences in chromosomal integrity and developmental outcome between these events should be determined. Nevertheless, a similar assessment of bovine blastocysts determined that micronuclei often reside in the placental-derived TE, but can also be contained within the ICM of the embryo, where they may be less tolerated.

Given the large range in the percentage of aneuploidy (~32-85%) and differences in the whole-genome method used in previous studies (Destouni et al., 2016; Hornak et al., 2016; Tsuiko et al., 2017), we sought to comprehensively assess the aneuploidy frequency in bovine embryos at multiple cleavage stages using an approach that provided uniform genome coverage and avoided the input of parental DNA (Borgstrom, Paterlini, Mold, Frisen, & Lundeberg, 2017; de Bourcy et al., 2014); (McCoy, Demko, Ryan, Banjevic, Hill, Sigurjonsson, Rabinowitz, Fraser, et al., 2015; McCoy et al., 2018). After reconstructing each cleavage-stage embryo and combining the results, we determined that ~55% of the embryos contained only aneuploid cells, whereas another ~29% were mosaic, all of which were primarily the product of non-reciprocal mitotic errors. In those embryos with meiotic errors, most also

experienced mitotic missegregation of different chromosomes than those originally affected during meiosis and the remaining aneuploid embryos exhibited a complete loss and/or a gain of up to 6 copies of chromosomes characteristic of chaotic aneuploidy. This indicates that embryos with meiotic missegregation are more prone to mitotic errors and propagated by subsequent divisions, which helps explain the large genotypic complexity reported in human IVF embryos (Chavez et al., 2012; Chow et al., 2014; McCoy, Demko, Ryan, Banjevic, Hill, Sigurjonsson, Rabinowitz, Fraser, et al., 2015; Vanneste et al., 2009).

Because of apparent disparity on whether the MCC is functional in the early cleavage divisions of mammalian preimplantation development in previous studies (Vazquez-Diez et al., 2019b; Wei et al., 2011), we investigated the consequences of MCC inhibition by directly targeting BUB1B in bovine zygotes. Following injection, BUB1B MAO embryos either failed to divide even after several attempts or exhibited abnormal divisions that were multipolar and/or asymmetrical (**Fig. 6C**). Furthermore, immunostaining of the BUB1B MAO treated embryos that did divide revealed blastomeres with severely abnormal nuclear structures or those that were completely devoid of DNA. CNV analysis of blastomeres that did contain nuclear DNA showed chaotic aneuploidy, with a complete loss or excessive number of chromosomal copies as described in some uninjected embryos and recently reported in primate embryos with multipolar divisions (Daughtry et al., 2019). We speculate that without BUB1B, embryos were unable to obtain proper microtubule-kinetochore attachments prior to the first cytokinesis, resulting in failed SAC and arrest, or premature cell division and chromosome missegregation due to MCC dysregulation. The role of another SAC protein, Mad2, was also recently investigated in mouse embryos and while 40% Mad2 knockdown had no effect on blastocyst formation, it did increase the number of micronuclei present at the morula stage (Vazquez-Diez et al., 2019b). Both MAD2 and BUB1B bind CDC20 to prevent activation of the APC, but *in vitro* binding assays demonstrated that BUB1B is 12 times more effective than MAD2 in inhibiting CDC20 (Fang, 2002). In addition, it was shown in *Drosophila* that the recruitment of CDC20 to the kinetochore requires BUB1B and not MAD2 (Li, Morley, Whitaker, & Huang, 2010) and that BUB1B is maternally inherited (Perez-Mongiovi, Malmanche, Bousbaa, & Sunkel, 2005). Thus, these

studies help explain the robust effect of BUB1B deficiency observed here and suggests that inhibition of the MCC via BUB1B knockdown impacts early cleavage divisions in higher mammals by allowing multipolar cytokinesis and asymmetrical genome partitioning to occur.

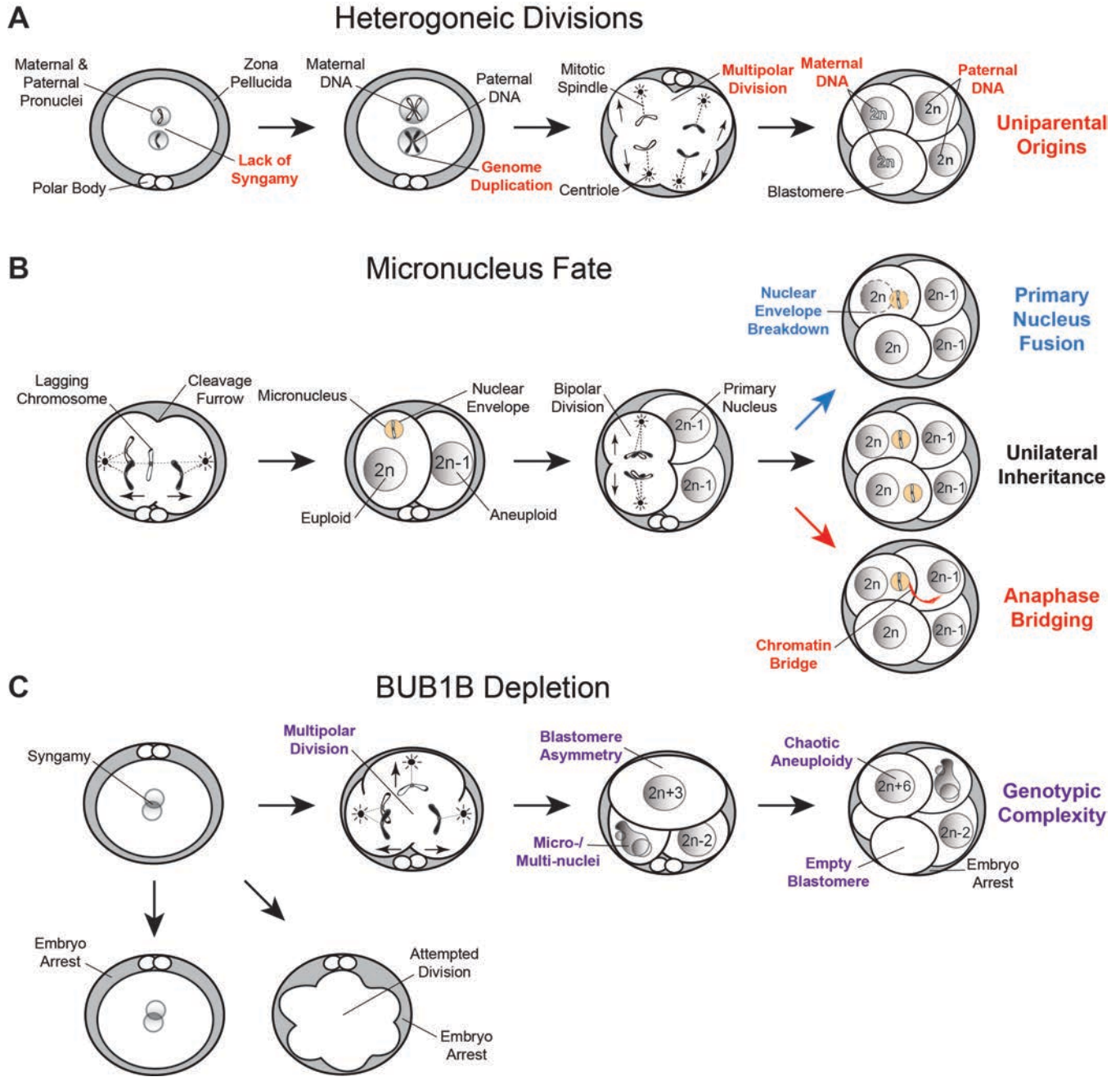


Figure 6. Summary of the major findings from the imaging, scDNA-seq, and gene knockdown studies. (A) Simplified model of how the lack of maternal and paternal pronuclear fusion (syngamy) at the zygote stage, followed by genome duplication and multipolar divisions, contributes to blastomeres with uniparental origins, or those that only contain maternal or paternal DNA. (B) Live-cell imaging also revealed the formation of anaphase lagging chromosomes likely from merotelic attachments prior to or during the first mitotic division. The chromosome(s) become encapsulated in nuclear envelope to form a micronucleus and the embryo continues to divide normally. In these subsequent bipolar divisions, most micronuclei either fuse back with the primary nucleus upon nuclear envelope breakdown or persist and undergo unilateral inheritance, but some micronuclei form a chromatin bridge with the nucleus of another blastomere during anaphase. (C) The depletion of BUB1B in zygotes resulted in no division or attempted division and embryo arrest, while multipolar divisions, blastomere asymmetry, and micro-/multi-nuclei were observed in BUB1B-deficient embryos that completed the first cytokinesis. These abnormal divisions also produced daughter cells with chaotic aneuploidy and/or empty blastomeres with no nuclear structure that induced embryo arrest and suggested that the lack of BUB1B permits the genotypic complexity detected at the early cleavage-stages of preimplantation development.

The expression of additional genes involved in mitosis and cell cycle progression was also affected by BUB1B knockdown and indicates that their abundance may be regulated by BUB1B availability in embryos. One of the downregulated genes included *Plk1*, which is conserved across both mammalian and non-mammalian species and has been shown to be important for the first mitosis in mouse zygotes (Ajduk, Strauss, Pines, & Zernicka-Goetz, 2017; Baran, Brzakova, Rehak, Kovarikova, & Solc, 2016). In somatic cells, PLK1 localization to non-attached kinetochores is required for the phosphorylation of BUB1B (Elowe, Hummer, Uldschmid, Li, & Nigg, 2007; H. Huang et al., 2008; H. Huang & Yen, 2009) and promotes the interaction of BUB1B with phosphatases that, in turn, inhibit excessive aurora kinase activity at kinetochores through positive feedback (Suijkerbuijk, Vleugel, Teixeira, & Kops, 2012). Therefore, the removal of BUB1B or inhibition of PLK1 increases the phosphorylation of kinase substrates, which has been shown to include *ECT2*, *POGZ*, and *HAUS6* (Bibi, Parveen, & Rashid, 2013; Kettenbach et al., 2011; Suzuki et al., 2015), genes identified as upregulated following BUB1B knockdown here. Since BUB1B MAO-injected embryos also exhibited increased expression of *CENP-F* and *SYCP3* and both are regulated by PLK1 phosphorylation in other contexts (Bisig et al., 2012; Santamaria et al., 2011), we suspect that these genes also serve as kinase substrates important for mitotic progression during embryogenesis. Additionally, we note that other polo-like kinase family members besides *PLK1* have been reported to play a role in tripolar divisions and aneuploidy in human embryos (McCoy, Demko, Ryan, Banjevic, Hill, Sigurjonsson, Rabinowitz, Fraser, et al., 2015;

McCoy et al., 2018) and determining how BUB1B cooperates with this regulatory network of kinases to reinforce SAC function and ensure chromosome fidelity during early mammalian embryogenesis requires further investigation. Overall, our results confirm a role for BUB1B and the MCC in maintaining proper chromosome segregation in initial cleavage divisions and show that the genotypic complexity observed in preimplantation embryos from higher-order mammals is likely contributed by deficiency in BUB1B or other maternally-inherited factors.

ACKNOWLEDGEMENTS

We gratefully acknowledge Dr. Tom Spencer at the University of Missouri-Columbia for the Madin-Darby Bovine Kidney (MDBK) epithelial cells. K.E.B. was supported by the NIH/NICHD Postdoctoral Individual National Research Service Award (5F32HD095550-01). B.L.D. was supported by the P.E.O. Scholar Award, N.L. Tartar Research Fellowship, and T32 Reproductive Biology NIH Training Grant (T32 HD007133). The authors acknowledge the support of the Oregon National Primate Research Center (ONPRC) Integrated Pathology Core for confocal microscopy (supported by S10RR024585) that operates under the auspices of the ONPRC NIH/OD core grant (P51OD011092). This work was supported by OHSU/ONPRC start-up funds (to SLC) and the NIH/NICHD (R01HD086073-A1). The content of this paper is solely the responsibility of the authors and does not necessarily represent the official views of the NIH.

AUTHOR CONTRIBUTIONS

Conceptualization, K.E.B. and S.L.C.; Methodology, K.E.B., B.L.D., and S.L.C.; Software, K.E.B., B.D., and M.Y.Y.; Validation, K.E.B. and S.L.C.; Formal Analysis, K.E.B. and S.L.C.; Investigation, K.E.B. and B.L.D.; Data Curation, S.S.F. and S.L.C.; Writing – Original Draft, K.E.B. and S.L.C.; Writing – Review & Editing, K.E.B., B.L.D., B.D., M.Y.Y., S.S.F., L.C., and S.L.C.; Visualization, K.E.B., B.D., and M.Y.Y.; Supervision, S.S.F., L.C., and S.L.C.; Project Administration, S.L.C.; Funding Acquisition, K.E.B., L.C., and S.L.C.

DECLARATION OF INTERESTS

The authors declare no competing interests.

MATERIALS AND METHODS

Reagents and media

All chemicals were obtained from Sigma-Aldrich (St. Louis, MO, USA) or Fisher Scientific (Pittsburgh, PA, USA) unless otherwise stated. Tyrode's albumin lactate pyruvate (TALP) medium with HEPES (TALP-HEPES) was used as washing media and contained 114mM NaCl, 3.2mM KCl, 25mM NaHCO₃, 0.34mM NaH₂PO₄-H₂O, 10mM C₃H₅NaO₃, 2 mM CaCl₂-H₂O, 0.5mM MgCl₂-6H₂O, 10.9 mM HEPES, 0.25mM sodium pyruvate, 1ul/ml Phenol Red, 3mg/ml FAF-BSA, 100uM Gentamicin Sulfate. For fertilization, TALP-IVF was used and comprised of 114mM NaCl, 3.2mM KCl, 25mM NAHCO₃, 0.34mM NaH₂PO₄-H₂O, 10mM C₃H₅NaO₃, 2mM CaCl₂-H₂O, 0.5mM MgCl₂-6H₂O, 1ul/ml Phenol Red, 0.25mM sodium pyruvate, 100units/ml penicillin, 100µg/ml streptomycin, 1uM epinephrine, 0.02 mM penicillamine, 10uM hypotaurine, 6mg/ml FAF-BSA, and 10mg/ml heparin.

IVF and embryo culture

Cumulus-oocyte complexes (COC) were retrieved by follicular aspiration of ovaries collected at a commercial abattoir (DeSoto Biosciences, Seymour, TN, USA). Those COCs with at least three layers of compact cumulus cells and homogeneous cytoplasm were placed in groups of 50 in 2ml sterile glass vials containing 1ml of oocyte maturation medium, covered with mineral oil, and equilibrated in 5% CO₂. Tubes with COCs were shipped overnight in a portable incubator (Minitube USA Inc., Verona, WI, USA) at 38.5°C. Following 24h of maturation, COCs were washed 3 times in TALP-HEPES followed by a final wash in fertilization media, before placement in a 4-well dish (Nunc™; Fisher Scientific) containing 0.5ml of fertilization media. Semen from either Racer (014HO07296) from Accelerated Genetics (Baraboo, WI, USA) or Colt P-red (7HO10904) from Select Sires (Plain City, OH, USA) was obtained for IVF. Sperm were purified from frozen-thawed straws using a gradient [50% (v/v) and 90% (v/v)] of Isolate (Irvine Scientific, Santa Ana, CA), washed two times in fertilization media by centrifugation at 100 RCF, and diluted to a final concentration of 1 million/ml in the fertilization dish. Fertilization was allowed to

commence for 17–19 h at 38.5°C in a humidified atmosphere of 5% CO₂. Presumed zygotes were denuded from the surrounding cumulus cells by vortexing for 4 min in 200µl of TALP-Hepes with 0.5% (w/v) hyaluronidase (Sigma-Aldrich). Denuded zygotes were washed in fresh TALP-Hepes prior to transfer to custom Eeva™ 12-well polystyrene dishes (Progyny, Inc., New York, NY; formerly Auxogyn, Inc.) containing 100µl drops of BO-IVC culture media (IVF Bioscience; Falmouth, Cornwall, UK) under mineral oil (CooperSurgical, Trumbull, CT) at 38.5°C in a humidified atmosphere of 5% CO₂, 5% O₂, and 90% N₂.

Time-lapse imaging

Zygotes were monitored with an Eeva™ darkfield 2.2.1 or bimodal (darkfield/brightfield) 2.3.5 time-lapse microscope system (Progyny, Inc) housed in a small tri-gas incubator (Panasonic Healthcare, Japan) as previously described (Vera-Rodriguez, Chavez, Rubio, Reijo Pera, & Simon, 2015). Images were taken every 5 min with a 0.6 second exposure time. Each image was time stamped with a frame number and all images compiled into an AVI movie using FIJI software version 2.0.0 (NIH, Bethesda, MD (Schindelin et al., 2012) for assessment of mitotic divisions by two independent reviewers.

Immunostaining and fluorescent imaging

Embryos were washed in PBS with 0.1% BSA and 0.1% Tween-20 (PBST; Calbiochem, San Diego, CA) and fixed with 4% paraformaldehyde (Alfa Aesar, Ward Hill, MA) in PBST for 20 min. at room temperature (RT). Once fixed, the embryos were washed with gentle shaking three times for a total of 15 min. in PBS-T to remove residual fixative. Embryos were permeabilized in 1% Triton-X (Calbiochem) for one hour at RT and washed in PBST as described above. To block non-specific antibody binding, embryos were transferred to a 7% donkey serum (Jackson ImmunoResearch Laboratories, Inc., West Grove, PA)/PBS-T solution for either 1 hour at RT or overnight at 4°C. An antibody against LMNB1 (catalog #ab16048, Abcam, Cambridge, MA) was diluted 1:1,000, while the CDX2 mouse monoclonal antibody (clone #CDX2-88, Abcam) was diluted 1:100 in PBS-T with 1% donkey serum, and embryos stained for 1 hour at RT or overnight at 4°C. Primary LMNB1 and CDX2 immunosignals were detected using 488-conjugated donkey anti-rabbit or 647-conjugated donkey anti-mouse Alexa Fluor secondary antibodies

(Thermo Fisher), respectively, at a 1:250 dilution with 1% donkey serum in PBS-T at RT for 1 hour in the dark. Embryos were washed in PBS-T and the DNA stained with 1 µg/ml DAPI for 15 min. Embryos were mounted on slides using Prolong Diamond mounting medium (Invitrogen, Carlsbad, CA, USA). Immunofluorescence was initially visualized on a Nikon Eclipse Ti-U fluorescent microscope system and images captured using a Nikon DS-Ri2 color camera and confirmed with a Leica SP5 AOBS spectral confocal system. Z-stacks, 1–5µm apart, were imaged one fluorophore at a time to avoid spectral overlap between channels. Stacked images and individual channels for each color were combined into composite images using FIJI software version 2.0.0.

Modified mRNA construction

Plasmids containing the coding sequence (CDS) for mCitrine-Lifeact (Addgene #54733), which labels filamentous actin (F-actin), mCherry-Histone H2B-C-10 (Addgene #55057), and mCherry-LAMINB1-10 (Plasmid #55069) were a gift from Dr. Michael Davidson's laboratory and deposited in Addgene (Cambridge, MA). Custom primers containing a 5'-T7 promoter sequence were used to amplify each fluorescent tag-mRNA fusion construct as follows:

T7_mCitrine_F: CTAGCTTAATACGACTCACTATAGGGCGGTGCGCCACCATGGTGA

LifeAct_R: TTAATTGTACAGCTCGTCCATGCCGAGAGTGATCCCGGC

T7_mCherry_F: AATTAATACGACTCACTATAGGGAGAGCCACCATGGTGAGCAA

H2B_R: GCGGCCGCTTTACTTGT

LAMINB1_R: TCCGGTGGATCCCTACATAA

PCR amplification was performed with high fidelity Platinum Taq polymerase (Thermo Fisher) under the following conditions: 94°C for 2 min., followed by 35 cycles of 94°C-30 sec., 70°C-30 sec. and, 72°C-3 min. PCR products were purified with the QIAquick PCR Purification kit (Qiagen; Hilden, Germany), then underwent *in vitro* transcription using the mMessage Machine T7 Transcription Kit (Invitrogen). Following the synthesis of capped mRNA, the MEGAclean transcription clean up kit (Invitrogen) was used to purify and concentrate the final modified mRNA product.

Live-cell imaging

Bovine zygotes were microinjected with mCitrine-Lifeact and either mCherry-H2B or mCherry-LAMINB1 mRNAs at a concentration of 20 ng/ul each in the presence of Alexa Fluor 488 labeled Dextran (Invitrogen) using a CellTram vario, electronic microinjector and Transferman NK 2 Micromanipulators (Eppendorf, Hauppauge, New York, USA). Zygotes that exhibited mCherry fluorescent signal within 4-6 hours following microinjection were selected for overnight imaging. Imaging dishes were prepared by placing 20 μ l drops of BO-IVC media on glass bottom dishes (Matek Corporation; Ashland, MA) and covering with mineral oil. A Zeiss LSM 880 laser-scanning confocal microscope with 10X objective and Fast Airy capabilities was used to capture fluorescent images of embryos for 18-20 hours, which encompassed the first three mitotic divisions. Z-stack images were taken every 1.5 μ m for a total of ~60 slices covering a 90 μ m range at 10 min. intervals. Each fluorophore was acquired independently to prevent crosstalk and maximize scanning speed. Individual images underwent Airyscan processing using Zeiss software and were compiled into videos with individual embryo labels using FIJI. Assessment of cytoplasmic and nuclear structure in embryos during mitotic divisions was completed by two independent reviewers.

Embryo disassembly

Embryos were disassembled under a stereomicroscope equipped with a heated stage and digital camera (Leica Microsystems, Buffalo Grove, IL) for documentation. The zona pellucida (Rocafort, Enciso, Leza, Sarasa, & Aizpurua) was removed from each embryo by a 30 second exposure to warm Acidified Tyrode's Solution (EMD Millipore, Temecula, CA), followed by 30-60 seconds in 0.1% (w/v) pronase (Sigma, St. Louis, MO, USA). Once ZP free, embryos were washed in TALP-Hepes and gently manipulated using a STRIPPER pipettor (Origio, Måløv, Denmark), with or without brief exposure to warm 0.05% trypsin- EDTA (Thermo Fisher Scientific, Waltham, MA) as necessary, until all blastomeres were separated. Following disassembly, each blastomere and cellular fragment if present was washed three times with Ca²⁺ and Mg²⁺-free PBS (Fisher Scientific), collected into individual PCR tubes in ~2 μ L of PBS,

and snap frozen on dry ice. Downstream analysis was completed only for embryos where the disassembly process was successful for all blastomeres.

DNA library preparation

Single blastomeres and cellular fragments underwent DNA extraction and WGA using the PicoPLEX single-cell WGA Kit (Rubicon Genomics, Ann Arbor, MI) according to the manufacturer's instructions with slight modifications. Cells were lysed at 75°C for 10 min. followed by pre-amplification at 95°C for 2 min. and 12 cycles of gradient PCR with PicoPLEX pre-amp enzyme and primer mix. Pre-amplified DNA was further amplified with PicoPLEX amplification enzyme and 48 uniquely-indexed Illumina sequencing adapters provided by the kit or custom adapters with indices designed as previously described (Vitek et al., 2017). Adapter PCR amplification consisted of a 95°C hotstart for 4 min., four cycles of 95°C for 20 sec., 63°C for 25 sec., and 72°C for 40 sec. and seven cycles of 95°C for 20 sec. and 72°C for 55 sec. Libraries were quantified with a Qubit High Sensitivity (HS) DNA assay (Life Technologies, Carlsbad, CA). Amplified DNA from each blastomere (50ng) and cellular fragment (25ng) was pooled and purified with AMPure® XP beads (Beckman Coulter, Indianapolis, IN). Final library quality assessment was performed on a 2200 TapeStation (Agilent, Santa Clara, CA).

Multiplex DNA-seq

Pooled libraries were sequenced on an Illumina NextSeq 500 using a 75-cycle kit with a modified single-end workflow that incorporated 14 dark cycles at the start of the first read prior to the imaged cycles. This step excluded the quasi-random priming sequences that are G-rich and lack a fluorophore for the two-color chemistry utilized by the NextSeq platform during cluster assignment. A total of $\sim 3.5 \times 10^6$ reads/sample were generated. All raw sample reads were demultiplexed and sequencing quality assessed with FastQC as previously described (Krueger, Andrews, & Osborne, 2011). Illumina adapters were removed from raw reads with the sequence grooming tool, Cutadapt (C. Chen, Khaleel, Huang, & Wu, 2014), which trimmed 15 bases on the 5' end and five bases from the 3' end, resulting in reads of 120 bp on average. Trimmed reads were aligned to the most recent bovine reference genome, BosTau8 (Zimin et al., 2009), using the BWA-MEM option of the Burrows-Wheeler Alignment Tool (Salavert Torres

J & J, 2012) with default alignment parameters. Resulting bam files were filtered to remove alignments with quality scores below 30 ($Q < 30$) as well as alignment duplicates that were likely the result of PCR artifacts with the Samtools suite (Ramirez-Gonzalez, Bonnal, Caccamo, & Maclean, 2012). The average number of filtered and uniquely mapped sequencing reads in individual libraries was between 1.9 and 2.2 million.

CNV analysis

CNV was determined by the integration of two previously developed bioinformatics pipelines, Variable Non-Overlapping Window Circular Binary Segmentation (VNOWC) and the Circular Binary Segmentation/Hidden Markov Model (CBS/HMM) Intersect termed CHI, as previously described (Vitak et al., 2017). All CNV calls from the two pipelines generated profiles of variable sized windows that were intersected on a window-by-window basis. Because other low-input sequencing studies have shown that CNV can be reliably assessed at a 15 Mb resolution with 0.5-1X genome coverage (Lee, Lee, Kim, & Yoon, 2013; Zhou et al., 2018), we classified breaks of 15 Mb in length or larger that did not affect the whole chromosome as segmental. Only whole and segmental CNV calls in agreement between the VNOWC and CHI methods at window sizes containing 4,000 reads were considered. Chaotic aneuploidy was classified by the loss or gain of greater than four whole and/or broken chromosomes as previously described (Delhanty, Harper, Ao, Handyside, & Winston, 1997). Additional classification of each aneuploidy as meiotic or mitotic in origin was accomplished by determining whether a loss or gain of the same chromosome was detected in all blastomeres (meiotic) or if different and/or reciprocal chromosome losses and gains were observed between blastomeres (mitotic).

Morpholino Design

Two non-overlapping MAOs were designed and synthesized by Gene Tools (Philomath, OR) to specifically target bovine BUB1B (Ensembl transcript ID: ENSBTAT00000009521.5). BUB1B MAO #1 (TTTCCTTCTGCATCGCCGCCATC) specifically targeted the ATG start codon of the BUB1B mRNA coding sequence, while BUB1B MAO #2 (CGATCTGAGGCTCTGAAGAAAGGCC) targeted upstream of MAO #1 in the 5' UTR of bovine *BUB1B*. A standard control MO (CCTCTTACCTCAGTTACAATTTATA)

that targets a splice site mutant of the human hemoglobin beta-chain (HBB) gene (GenBank accession no. AY605051) that is not present in the *Bos Taurus* genome served as a control. Both Bub1b and standard control MAO were synthesized with a 3'-Carboxyfluorescein tag to aid in visualization during embryo manipulation.

BUB1B knockdown

Zygotes underwent cytoplasmic injection with 3'-carboxyfluorescein-labeled MAO at 20 hours post fertilization as described above. A concentration of 0.3 mM MAO was used based on previous findings that standard control MAO at this concentration was the maximum which allowed normal blastocyst formation rates (Foygel et al., 2008). Following microinjection, embryos were cultured up to the blastocyst stage as described above with or without imaging on the Eeva™ darkfield 2.2.1 microscope system. Upon developmental arrest, embryos were collected for immunostaining, gene expression analysis, or disassembled into single cells (as described above) for downstream analysis.

Validation of BUB1B knockdown

To further validate MAO specificity, bovine embryos were co-injected with BUB1B modified mRNA at a concentration of approximately 3 nl (75 pg) of mRNA per embryo in addition to BUB1B MAO #1. The BUB1B coding sequence (CDS) was amplified from the plasmid, pcDNA5-EGFP-AID-BubR1 (Addgene #47330), followed by mutation of the MAO binding site using the Q5 site directed mutagenesis kit (NEB) according to the manufacturer's instructions. Briefly, custom primers (forward: 5'-aaaaaagaggggaGGTGCTCTGAGTGAAGCC-3', and reverse: 5'-aactgcagccatATGGGATCCAGCTCTGCT-3') were designed to mutate the region of the BUB1B CDS targeted by the MAO without affecting the amino acid sequence. Exponential amplification of the template plasmid using high fidelity DNA polymerase was followed by a single step phosphorylation, ligation and DpnI restriction enzyme digestion. NEB 5- α competent cells were transformed with the mutated plasmid, followed by DNA miniprep isolation using QIAprep spin columns (Qiagen). Mutated plasmids were identified by Sanger sequencing performed by the ONPRC Molecular and Cellular Biology Core using a custom designed primer (TTGGTGAATAGCTGGGACTATG). Following identification and

isolation, the mutated plasmid served as a template to synthesize a PCR product containing a T7 promoter using Platinum Taq (Invitrogen). Custom primers (forward: CTAGCTTAATACGACTCACTATAGGGAGCGCCACCATGGCTGCAGTTAAAAAAGAG, reverse: CAATCTGTGAGACTTGATTGCCTAGCTCACTGAAAGAGCAAAGCCCCAG) were designed for use with the T7 mMessage mMachine Ultra Kit as described above.

Quantitative RT-PCR analysis

Gene expression was analyzed in Std control MAO and BUB1B MAO injected embryos using the BioMark Dynamic Array microfluidic system (Fluidigm Corp., So. San Francisco, CA, USA). All embryos were collected within 36 hours post fertilization as described above. Individual embryos were pre-amplified according to the manufacturer's "two-step single cell gene expression" protocol (Fluidigm Corp.) using SuperScript VILO cDNA synthesis kit (Invitrogen), TaqMan PreAmp Master Mix (Applied Biosystems, Foster City, CA, USA), and gene-specific primers designed to span exons using Primer-BLAST (NCBI). Bovine fibroblasts and no RT template samples were used as controls. Pre-amplified cDNA was loaded into the sample inlets of a 96 × 96 dynamic array (DA; Fluidigm Corp.) and assayed in triplicate. A total of 10 reference genes were assayed for use as relative expression controls. Cycle threshold (Ct) values were normalized to the two most stable housekeeping genes (*RPL15* and *GUSB*) using qBase⁺ 3.2 software (Biogazelle; Ghent, Belgium). Calculated normalized relative quantity (CNRQ) values were averaged across triplicates \pm the standard error and graphed using Morpheus (<https://software.broadinstitute.org/morpheus/>).

Statistical Analysis

Averaged CNRQ values of each gene was compared across embryo groups using the Mann-Whitney U-test. The unadjusted p-value ≤ 0.05 was considered statistically significant.

SUPPLEMENTAL INFORMATION

Genotypic Complexity in Initial Cleavage Divisions of Mammalian Embryos is Contributed by Defective BUB1B/BUBR1 Signaling

Kelsey E. Brooks¹, Brittany L. Daughtry^{1,2}, Brett Davis^{3,4}, Melissa Y. Yan³, Suzanne S. Fei³, Lucia Carbone⁴⁻⁷, Lina Gao³, Byung Park³, and Shawn L. Chavez^{1,7-9*}

¹Division of Reproductive & Developmental Sciences, Oregon National Primate Research Center, Beaverton, Oregon 97006, USA

²Department of Cell, Developmental & Cancer Biology, Oregon Health & Science University, Portland, Oregon 97239, USA

³Bioinformatics & Biostatistics Core, Oregon National Primate Research Center, Beaverton, Oregon 97006, USA

⁴Department of Medicine, Knight Cardiovascular Institute, Oregon Health & Science University, Portland, Oregon 97239, USA

⁵Division of Genetics, Oregon National Primate Research Center, Beaverton, Oregon 97006, USA

⁶Department of Medical Informatics and Clinical Epidemiology, Division of Bioinformatics & Computational Biomedicine, Oregon Health & Science University, Portland, Oregon 97239, USA

⁷Department of Molecular and Medical Genetics, Oregon Health & Science University, Portland, Oregon 97239, USA

⁸Department of Obstetrics & Gynecology, Oregon Health & Science University, Portland, Oregon 97239, USA

⁹Department of Biomedical Engineering, Oregon Health & Science University, Portland, Oregon 97239, USA

*Corresponding Author: chavesh@ohsu.edu

Supplemental Methods

Madin-Darby Bovine Kidney (MDBK) cell culture

The Madin-Darby Bovine Kidney (MDBK) epithelial cell line (Madin & Darby, 1958) was a kind gift from Dr. Thomas Spencer at the University of Missouri-Columbia. Cells were cultured in Eagle's Minimum Essential Medium modified to contain Earle's Balanced Salt Solution, non-essential amino acids, 2 mM L-glutamine, 1 mM sodium pyruvate, and 1500 mg/L sodium bicarbonate, 10% (v/v) FBS and antibiotics (50 U penicillin, 50 µg streptomycin) in 5% CO₂ at 37°C.

Assessment of BUB1B MAO knockdown

MDBK epithelial cells were plated on poly-L-lysine treated coverslips, and grown to 70% confluency prior to MAO treatment. Cells were incubated with 6 µl/ml Endo-Porter delivery reagent containing DMSO (Gene Tools) and 2, 4, or 8 µM of either Bub1b MAO #1 or Standard control MAO. After 36 hours, cells were synchronized at metaphase in the presence of 0.03µg of colcemid (Sigma) for 12 hours, and collected for staining at 48 hours post MAO treatment. Cells were washed in PBS, followed by a single 20 min. fixation and permeabilization step using 4% paraformaldehyde (Alfa Aesar, Ward Hill, MA) with 1% Triton-X (Calbiochem) in PBS. Additional PBS washes were completed prior to blocking with 7% donkey serum (Jackson ImmunoResearch Laboratories, Inc., West Grove, PA) in PBS for either 1 hour at RT or overnight at 4°C. A primary antibody against Bub1b (ab28193, Abcam, Cambridge, MA) was diluted 1:1000 in PBS with 1% donkey serum and cells were incubated overnight at 4°C. Bub1b antibody binding was detected using a 568- conjugated donkey, anti-rabbit Alexa Fluor secondary antibody (Thermo Fisher) at a 1:250 dilution with 1% donkey serum in PBS at RT for 1 hour in the dark. Cells were washed in PBS and the DNA stained with 1 µg/ml DAPI for 15 min. The coverslips with adherent cells were then mounted on slides using Prolong Diamond mounting medium (Invitrogen, Carlsbad, CA, USA). Immunofluorescence was visualized on a Nikon Eclipse Ti-U fluorescent microscope system. Bub1b immunostaining was assessed visually for 100 metaphase cells in each MAO concentration treatment group. To determine statistical differences between treatment concentrations log-binomial modeling using the Generalized Estimating Equations (GEEs) approach was performed, and Tukey adjusted p-

values reported to adjust for multiple comparisons. Representative fluorescent images were captured using a Nikon DS-Ri2 color camera. Using FIJI, background fluorescence was subtracted from the red (BUB1B) channel, followed by combination of individual channels for each color into a composite image.

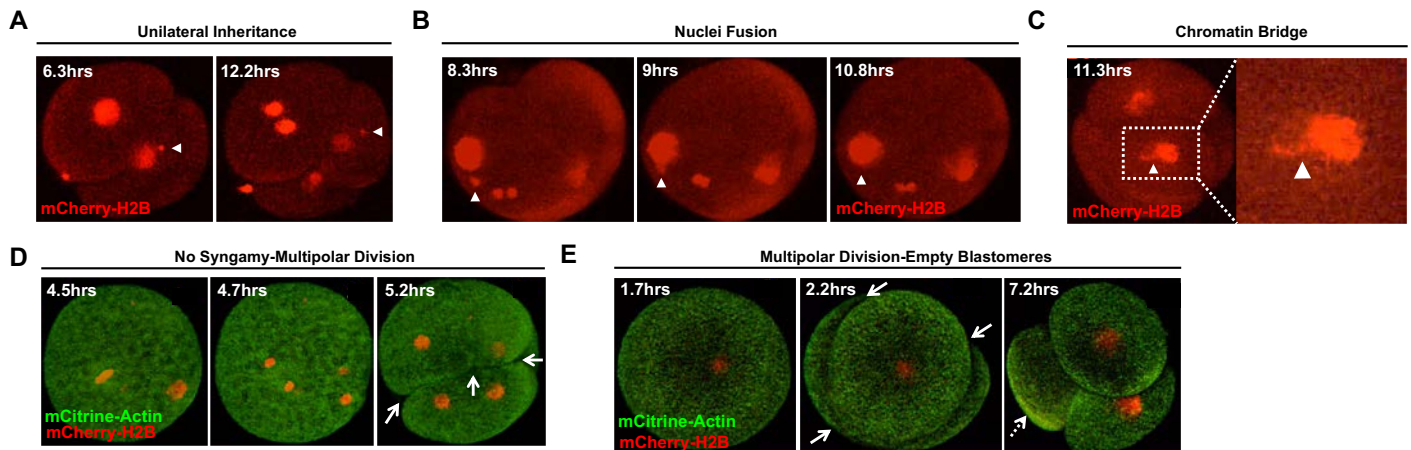
Supplemental Tables

Supplemental Table S1. Sequencing statistics of all embryonic and control samples. A table depicting the number or percentage of reads following de-multiplexing of embryonic (with embryo stage) and fibroblast samples at each step of the post-sequencing process, including adaptor removal, repeat masking, genome mapping, and quality assessment. The sequencing kit used and whether single- or paired-end is also included.

Supplemental Table S2. List of all genes with primers analyzed by qRT-PCR in zygotes. A table of the genes analyzed by microfluidic RT-qPCR in non-injected bovine zygotes and following Std Control MAO versus BUB1B MAO #1 microinjection. Included is the sequence of the forward and reverse primer used for amplification as well as the NCBI accession number of each gene.

Gene Symbol	Forward primer sequence (5'→3')	Reverse primer sequence (5'→3')	NCBI Accession #
ACTB	CCTTCTGGGCTGGAATCCT	GGCTTTTGGGAAGGCAAAAGG	NM_173979.3
ADAMTS18	GCAGCGGATTAACCACGATTA	ATCGGTAATGACGGGAGCTG	NM_001192486
ADAMTS20	CAGGCAGGAAGCCCTTAGTGA	TCTGTGGGAATACCTTCGCCG	NM_001206093
ANAPC10	AACAGATTCCCTTGGCGGAG	CCACCAATTC AAGTGGCCGA	NM_001080357.2
ANAPC2	GTATTTCCAGGACCAAGCCAGC	GCGGCTCAGCCACAACCTCT	XM_003584964.2
APBB1	GATGAGACGCTGAAGCTGGT	ACGTAGGCAAACTCCCTCC	NM_001075186
ATM	GCCAGAAATGTGAGCAACACC	AGCCAAGAACACCCACCAAA	NM_001205935.1
AURKA	AGCATGGATGAGTGGGTGAAT	TCTGTCCATGATGCCTGAGTC	NM_001038028.1
AURKB	TCCGACCCCTTACTCTCTCTC	AGGAACGCTTTGGGATGTTG	NM_183084.2
B2M	GCACCATCGAATTTGAACATT	GCAGAAGACACCCAGATGTTG	NM_173893
BAD	TCAGGGCCCTCATTTATCGGG	GGAAAGCCCTTGAAGGAGAGC	NM_001035459.1
BAX	TAAACATGGAGCTGCAGAGGATGA	CAGCAGCCCTCTCGAA	NM_173894.1
BCL2	GAGGCTGGGACGCCCTTGT	GGCTTACATGATGCCCCAGAT	NM_001166486.1
BRCA1	CCTACCTTGCAGGAAACCAGT	AATTGGCTTGGCCTTGGCT	NM_178573.1
BRCA2	AGTTTCCGCTGTCTTCTCCC	GGTTTCTGTGCCTTTGCGAG	XM_002684277.2
BUB1	GCAGCTGGTGATAAAGGGGAA	AAAATCCGATTCTCCGCGA	NM_001102011.2
BUB1B	AGCTACAAGGGCAGTGACC	CTTTGTCCCTTTATCACCAGC	NM_001145173.1
BUB3	ATGGGACACGCTTTCGAATA	TGGTTAGGTGACTTGGGTT	NM_001076177.1
CASP2	CTGTAGTCCCGCGTTGAG	CATCGCTCTCTCGCATTTG	NM_001144104.1
CASP3	ACGAAATACTGGCATGGCCT	TCCGTTCTTTGCATTTGCC	NM_001077840.1
CCNA1	CCTCACCTTACCCCCAGA	GCTTACTGCTCTGGTTGAGT	XM_005194120.1
CCND1	AGATGTGACCCGACTGCC	GGAAAACACCCAGACAGTGA	NM_001046273.2
CCNE1	TTGCTGCTTCCGCTTTGTAT	TTGCTTGGGCTTTGTCCAGC	NM_001192776.1
CD81	ATTTCTGCTTCTGGCTGCCA	CGATAAGGATGTAGATGCCACA	NM_001035099
CDC20	TGGAGCGGCGAGTTTAAGTT	CCATGGGAACCTGCTCAGT	NM_001082436.2
CDH18	AATGAAGATAACACGCCAGCA	TGCTGAGAGAGGGGATTTCCA	NM_001076837
CDK1	GCGGATAAAGCCGGGCTCT	GCTCTGGCAAGGCCAAAATC	NM_174016.2
CDK2	ATACACTGGCTTCCATCCCG	TACCACAGATCACACCTCG	NM_001014934.1
CDKN1A	GGAGACCGTGGTTGGGAGA	CGTTGGAGTGGTGAATACTGT	NM_001098958.2
CDX2	ACGTGAGATGTATCCACGC	TTCTTTGCTCTGCGGGTCT	NM_001206299.1
CENPE	CCGTGGAGGTTTCTGACGTA	CAGGCGCTTCTTCTCTGTGA	XM_010805939.3
CENPF	CCTATTGCGGGAAAAAGAGCA	CTCGTTTACGTTTACGCTTTTTCAG	NM_001256586.1
CENTRIN2	CGTCCGGGATGGCCTCTAA	AATGGCAGGCACTAAACCGA	NM_001038515.1
CHEK1	CAACTTATGCGAGGGGTGGT	ATGTAGCAGAGCTAGAGGAGC	NM_001098023.1
CHEK2	GGGTTTATCGCCAATCCGCT	ACCCATTTCTCTGAAGATCCGAAA	NM_001034531.1
CREBBP	CAAACCTGGAGGCGAGCAGAT	CATCTGAGGCATGTTGGCA	NM_001164022.1
CRTAC1	GACAAGCCCGTGTGTGCAA	AAGGAGTGAAGGAGGCCACA	NM_001205325
CSPP1	TCCCITTCCTATTGGTGAAGGT	GTCTGTTCCCGTACATCTGTT	NM_001193015.2
CTNNB1	AGAACAACAAATGACGTGGAGA	GACCTTCCATCCCTCTCTGTT	NM_001076141.1
CYP3A7-3A51P	GGCCATGGAGCTAATCCTGA	TCCATATAGATAGAGGACCCAGA	NM_001099367
DIAPH1	CACAGCAACGCAAACTGG	TTGAGGGAGACACGAAGGGA	XM_001787599.3
DYSF	ATGTGGTGCACCTGTTTCC	CGCAGSAAAAACCTTCTGGC	NM_001102490
ECT2	ACGAGAGACAGAAAGATTGCCA	GAGTATGTGAACCAAGAACCCA	NM_001097573.1
EOMES	GACAACATGATTCATCCATCAGA	TGATGGATGGGGTGTCTCT	NM_001191188.1
ERLEC1	GCCAGTCACTACAGGATCG	CCACCAACCAACACCCCTTT	NM_001191407.1
FSD1	AAAGTCAAAGTTGGAACGGCT	CCAGCGCTTGAACCCATTAC	NM_001081518
FZD2	TCCACGAGAGAAAGGCGATA	CCCAGAAGTTTGGGCATGAT	XM_003587455.5
GSG2	ACAACAACCTGCTGGGTGAA	CTTCAAGGCGGGGTGTTAT	NM_001076544
GUSB	TCCGACAGGCAAGAAATCAC	TGGCAATCAGCGCTTTGAA	NM_001083436
HAGHL	CTGCCCTTGAGACAAAGG	TGGTCTGTGAAGGCTCCAC	NM_001075540
HAUS6	AGGTATCAAAATGGGATTTGGCA	ATGCCACTGTGCATAGGACT	XM_002689566.6
INCEP	AGAACGCTTTCGCGAGAAGAA	GTCTTTCTGCGGGACAACCT	XM_584352.7
IQCG	CGACCTACGCTTTCAGTACC	GGCTTCCAGACCTTCTTCCA	NM_001038195
KAT2A	TGTGAGCACCTTTCGGCTGA	AACGAGCCTTACTTTGGGGAAG	XM_001788901.3
KAT2B	TTGGGTGGGAAGTTTCTG	TTCTGGTCCAGCGCTTGAAG	XM_613744.7
KCTD1	AATGGGCACAGAACGAGCAA	ATATTGGCCGACTGTCTGG	NM_001080360
KNL1	CGCGAGTAACTTCTGCTCT	AAACTTTTCTGAGCCACGCG	XM_002690821.6
MAD2L1	GAGAGGCTCTTGAAGATGGCA	AGACTTTTCTGGGTGCCACTAT	NM_001191513.1
MAP2K6	TTGACATGAAGTTTCCACGCC	TGCTTTCTGCTTTCGCACT	NM_001034045
MCL1	CGGTGATTGGCGGAAGCG	AACCCATCCAGCCTCTTTGTT	NM_001099206.1
MIS18A	TGCATCTTGTACGCTGTGT	GTTGAGCGAATCCTGTGTC	NM_001098010
MYH2	AAGAGCCCTTGGAAATGAGGC	GCTGAACCTCAGAGGCTTGT	NM_001166227
NANOG	CGGACACTGTCTCTCTCTC	CCATTGCTATTCTCTGGCCA	NM_001025344.1
NPM2	GTGCTGTTGCTCAGTACGATT	ATGGTGTCTTACTGCTCTCTC	NM_001168708.1
OEEP	CGCCCGAGCTGAGAAAATGG	GGTGGGAAAGGACAGAGATT	NM_001077869.2
PLK1	GTATGGCCTCGGATATCAGC	TCCGCTCCTGATGACTGTAG	NM_001038173.2
POGZ	ACTACTACAGCTGGCAATCTT	ATGGGCGAGGCTCACTAGTTG	NM_001163190.1
PPIA	GGATTTATGTGCCAGGGTGGTGA	CCAGGACCTGTATGCTTCAAAATG	NM_178320.2
PPP1CA	TGCCAAGAGACAGTGTGTGA	TGCCATACTTGCCTTATTCT	NM_001035316.2
PRKCQ	CCCAACCTTCTGTGAGCACT	CATTCATGCCACATGCGTCC	NM_001192077
PRKRIP1	AGAACTGGCTGCACTCCCA	GCAGTCAGCTCCTCCACATC	NM_001079841
RCC2	CTCTCATCACACGGAAGG	CAGGACCAGCGTGTGGTTAG	NM_001101911.2
ROBO2	ACAGATGATCTTCCACCCACAC	AAGTTGGCTGCTTGTGCT	XM_024993907.1
RPL15	GGCAGCCATCAGGGTGGG	CATCACGCTCCGACTGCTTCT	NM_001077866.1
RPS6K1	GTTCAGACACAGCCAAAGGACC	ACAGAGCGCCCTTGAGTGAC	NM_001083722.1
RPS6KA5	ACCCCTTCTTCCAGGGTCTG	CAGGCTCCAGTCCGGTAAAT	NM_001192023.1
RSP6KA4	CACCTTCTACTAGCTGCCCC	TTGTTGAAGGCGTGGAAAAGTG	NM_001191400.1
SCPEP1	ACACATGGTCTTCCGACC	CAGCCAGGCCATCCTATTCT	NM_001045909
SDHA	TCCTGCAGACCCGGAGATAA	TCTGCATGTTGAGTCGCACT	NM_174178
SEPT6	CCGATATAGCTCGCCAGGTG	CCAAAACCTGTCTCTCCACG	NM_001035430
SIRT2	GTCACGGGATAGAGAGTCCG	TCTGAGTCTGAGCCTCTGCT	NM_001113531.1
SMIM8	GCCTTTAAAAAGGAGCCGCC	AAGCCATTACAGGTTTGTAGGT	NM_001081531
SMTN	GTTCTACCGCTGTCTGGTCC	CAGTCCACCAGCATCCGCTG	NM_001076879
SPICE1	GCTATCGGAAACGCAAGATGT	CGCCTGCGAGGAAAATCAAC	NM_001038117.2
STX3	TTTAGCAACTGAGCGAACAGG	CATACCCTTATCCCTCTGCG	NM_001101971
SYCP1	CCCGCTTTTCCGAGTAGAT	TCCTCCGAAAGTCTGAGGTT	XM_003581953.2
SYCP3	CCAACAAGAGCAAGGCAAGAG	TGCTGCTGTTACATGAGAGAAGAT	NM_001040588.2
SYT1	GACCATGAAAGATCAGGCC	CAGCAGCTGGTTATTCTGGA	NM_174192
SYT2	CTTGGCGAAAGACACTCC	CAGAGGACAGCGGGGT	XM_024976596.1
TBC1D7	CGGACTTGGCTTAGGACTC	CAACTCCAGAAACCCCACT	NM_001015643
TEX14	ACGAAGTCTTGAAGGCGAAC	GATGGCTTCTACAGGATCTTTCG	NM_001192568.1
TUBA1C	TTCTCCCCGACTCCTTAG	ATGCACTCACGCATAACGGA	NM_001034204
TUBG1	ACCAGCATCTCCTCGCTCTT	CAGTAAGGCAAGTGAAGGCTCC	XM_001790429.3
UBC	GTCCGAGCCGGGAGTTC	TCACAAAGATCTGCATTTGCAATTA	NM_001206307.1
WRAP73	GTAACCTGGCTTCTGCATCC	CACCTCAGGCTGCTGGATCTG	NM_001193006
YWHAZ	ACCTACTCCGACACAGAACA	ATCATATCGCTCAGCCTGCTC	NM_174814

Supplemental Figures



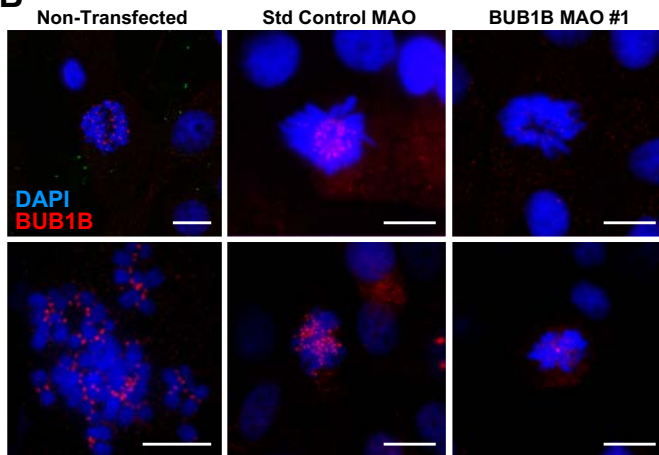
Supplemental Figure S1. Additional live-cell images representative of embryos with different phenotypes. Live-cell confocal microscopy of bovine zygotes microinjected with fluorescently labeled modified mRNAs to visualize DNA (Histone H2B-mCherry; red) and distinguish blastomeres (Actin-mCitrine; green) during the first three mitotic divisions. **(A)** Examples of other embryos with micronuclei that undergo unilateral inheritance, **(B)** fuse back with the primary nucleus, or **(C)** form a chromatin bridge (white arrowheads). **(D)** Images of additional embryos that bypassed pronuclear fusion (syngamy) prior to a multipolar division (white solid arrows) to produce blastomeres with uniparental origins and/or **(E)** no apparent nuclear structure (white dashed arrows). Individual frames are represented in hours (hrs) from the start of imaging.

A

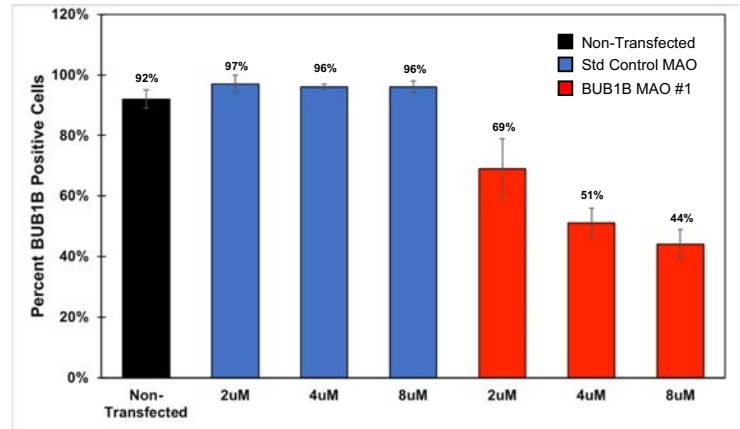
BUB1B targeting sequences: (BUB1B MAO #1; BUB1B MAO #2)

5'-GTTGCAGAAGGAGGCCAGG[CGATCTGAGGCTCTGAAGAAAGGCC]CGC...
...GGGAGGACGAGGCCCTGAGCCGGGAATGCAG[G(ATG)CGGCGATGCAGAAGGAAA]GGG- 3'

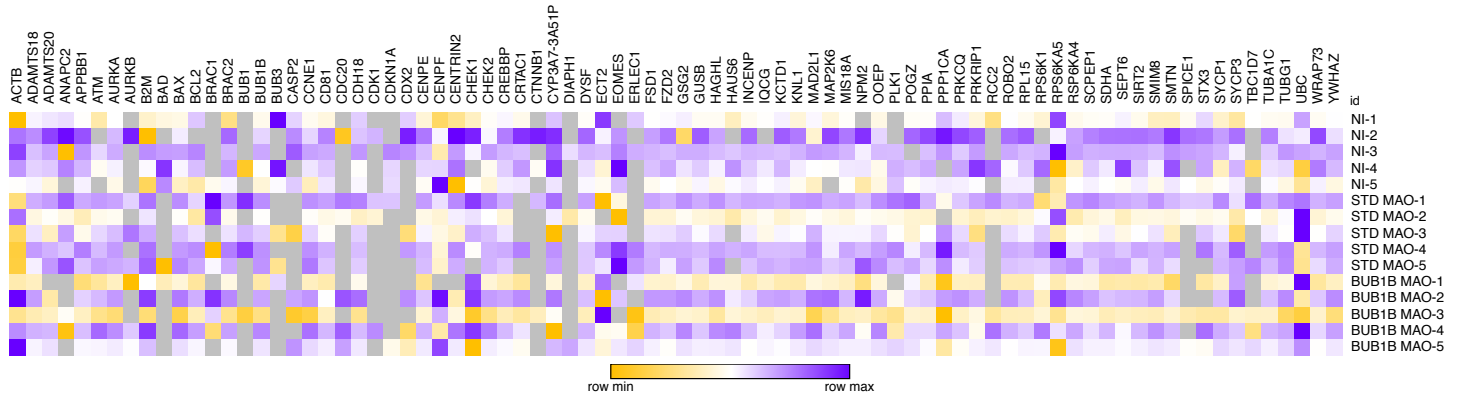
B



C



Supplemental Figure S2. BUB1B MAO design and knockdown efficiency. (A) DNA sequences of two non-overlapping MAOs designed to target the ATG start site (shown in red, BUB1B MAO #1) and the 5' UTR (depicted in blue, BUB1B MAO #2) of BUB1B. (B) BUB1B knockdown efficiency was assessed in synchronized MDBK cells following 48 hours of treatment with 3 μl/ml of colcemid alone (non-transfected), the Std control MAO, or BUB1B MAO #1 via immunofluorescence. BUB1B protein expression was analyzed in DAPI stained (blue) MDBK cells. Note the lack of or reduced number of BUB1B positive foci (red) in the BUB1B MAO #1 treated cells compared to the controls; Scale bar = 20 μm. (C) Bar graph showing the percentage of MDBK cells in metaphase with BUB1B expression after colcemid treatment (black) or transfection with different concentrations (2, 4, and 8 μM) of the Std control MAO (blue) or BUB1B MAO #1 (red). While the number of cells exhibiting BUB1B positive foci was similar between the non-transfected and Std MAO controls, a dose-dependent decrease in BUB1B expression was observed following BUB1B MAO #1 treatment.



Supplemental Figure S3. Comprehensive assessment of gene expression patterns in zygotes. Heat map of all mitotic, cell cycle, developmentally-regulated, and cell survival genes assessed in individual BUB1B MAO #1 versus non-injected and Std Control-injected MAO bovine zygotes via microfluidic qRT-PCR. Cycle threshold (Ct) values were normalized to the most stable reference genes (RPL15 and GUSB) across embryo groups and presented as the average. Gray squares indicated no expression, whereas yellow, white, and purple squares correspond to low, medium, and high expression, respectively.

Supplemental Movies

Supplemental Movie S1. Live-cell fluorescent imaging of early cleavage divisions. Bovine zygotes were microinjected with fluorescently labeled modified mRNAs to mCitrine-Actin (green) and mCherry-Histone H2B (red) to distinguish blastomeres and DNA, respectively, and early mitotic divisions visualized by live-cell confocal microscopy. Note the micro-/multi-nuclei in embryos #3, #4, and #11, chromatin bridge in embryo #1, lack of syngamy in embryos #3 and #11, multipolar divisions in embryos #1, #3-6, #11, and #15, and production of empty blastomeres in embryos #5 and #15.

Supplemental Movie S2. BUB1B deficient embryos struggle to divide. A bovine zygote following BUB1B MAO microinjection attempts to divide by forming multiple cleavage furrows, but never successfully completed cytokinesis.

Supplemental Movie S3. Multipolar divisions are observed in BUB1B-injected embryos. Certain bovine zygotes were able to undergo cytokinesis even with BUB1B knockdown, but these divisions were abnormal with multipolar cleavage.

Supplemental Movie S4. BUB1B knockdown causes blastomere asymmetry. Besides abnormal divisions, BUB1B-injected bovine embryos often exhibited blastomere asymmetry following the multipolar cleavage.

REFERENCES

- Ajduk, A., Strauss, B., Pines, J., & Zernicka-Goetz, M. (2017). Delayed APC/C activation extends the first mitosis of mouse embryos. *Sci Rep*, 7(1), 9682. doi:10.1038/s41598-017-09526-1
- Alper, M. M., Brinsden, P., Fischer, R., & Wikland, M. (2001). To blastocyst or not to blastocyst? That is the question. *Hum Reprod*, 16(4), 617-619. doi: 10.1093/humrep/16.4.617
- Baker, D. J., Jeganathan, K. B., Cameron, J. D., Thompson, M., Juneja, S., Kopecka, A., . . . van Deursen, J. M. (2004). BubR1 insufficiency causes early onset of aging-associated phenotypes and infertility in mice. *Nat Genet*, 36(7), 744-749. doi:10.1038/ng1382
- Baran, V., Brzakova, A., Rehak, P., Kovarikova, V., & Solc, P. (2016). PLK1 regulates spindle formation kinetics and APC/C activation in mouse zygote. *Zygote*, 24(3), 338-345. doi:10.1017/S0967199415000246
- Bibi, N., Parveen, Z., & Rashid, S. (2013). Identification of potential Plk1 targets in a cell-cycle specific proteome through structural dynamics of kinase and Polo box-mediated interactions. *PLoS One*, 8(8), e70843. doi:10.1371/journal.pone.0070843
- Bisig, C. G., Guiraldelli, M. F., Kouznetsova, A., Scherthan, H., Hoog, C., Dawson, D. S., & Pezza, R. J. (2012). Synaptonemal complex components persist at centromeres and are required for homologous centromere pairing in mouse spermatocytes. *PLoS Genet*, 8(6), e1002701. doi:10.1371/journal.pgen.1002701
- Bolton, H., Graham, S. J., Van der Aa, N., Kumar, P., Theunis, K., Fernandez Gallardo, E., . . . Zernicka-Goetz, M. (2016). Mouse model of chromosome mosaicism reveals lineage-specific depletion of aneuploid cells and normal developmental potential. *Nat Commun*, 7, 11165. doi:10.1038/ncomms11165
- Borgstrom, E., Paterlini, M., Mold, J. E., Frisen, J., & Lundeberg, J. (2017). Comparison of whole genome amplification techniques for human single cell exome sequencing. *PLoS One*, 12(2), e0171566. doi:10.1371/journal.pone.0171566
- Braude, P., Bolton, V., & Moore, S. (1988). Human gene expression first occurs between the four- and eight-cell stages of preimplantation development. *Nature*, 332(6163), 459-461. doi:10.1038/332459a0
- Chavez, S. L., Loewke, K. E., Han, J., Moussavi, F., Colls, P., Munne, S., . . . Reijo Pera, R. A. (2012). Dynamic blastomere behaviour reflects human embryo ploidy by the four-cell stage. *Nat Commun*, 3, 1251. doi:10.1038/ncomms2249
- Chen, C., Khaleel, S. S., Huang, H., & Wu, C. H. (2014). Software for pre-processing Illumina next-generation sequencing short read sequences. *Source Code Biol Med*, 9, 8. doi:10.1186/1751-0473-9-8
- Chen, S., Takanashi, S., Zhang, Q., Xiong, W., Zhu, S., Peters, E. C., . . . Schultz, P. G. (2007). Reversine increases the plasticity of lineage-committed mammalian cells. *Proc Natl Acad Sci U S A*, 104(25), 10482-10487. doi:10.1073/pnas.0704360104
- Chow, J. F., Yeung, W. S., Lau, E. Y., Lee, V. C., Ng, E. H., & Ho, P. C. (2014). Array comparative genomic hybridization analyses of all blastomeres of a cohort of embryos from young IVF patients revealed significant contribution of mitotic errors to embryo mosaicism at the cleavage stage. *Reprod Biol Endocrinol*, 12, 105. doi:10.1186/1477-7827-12-105
- Crasta, K., Ganem, N. J., Dagher, R., Lantermann, A. B., Ivanova, E. V., Pan, Y., . . . Pellman, D. (2012). DNA breaks and chromosome pulverization from errors in mitosis. *Nature*, 482(7383), 53-58. doi:10.1038/nature10802
- Daughtry, B. L., Rosenkrantz, J. L., Lazar, N. H., Fei, S. S., Redmayne, N., Torkenczy, K. A., . . . Chavez, S. L. (2019). Single-cell sequencing of primate preimplantation embryos reveals chromosome elimination via cellular fragmentation and blastomere exclusion. *Genome Res*, 29(3), 367-382. doi:10.1101/gr.239830.118
- de Bourcy, C. F., De Vlaminck, I., Kanbar, J. N., Wang, J., Gawad, C., & Quake, S. R. (2014). A quantitative comparison of single-cell whole genome amplification methods. *PLoS One*, 9(8), e105585. doi:10.1371/journal.pone.0105585

- Delhanty, J. D., Harper, J. C., Ao, A., Handyside, A. H., & Winston, R. M. (1997). Multicolour FISH detects frequent chromosomal mosaicism and chaotic division in normal preimplantation embryos from fertile patients. *Hum Genet*, 99(6), 755-760. doi: 10.1007/s004390050443
- Destouni, A., Zamani Esteki, M., Catteeuw, M., Tsuiko, O., Dimitriadou, E., Smits, K., . . . Vermeesch, J. R. (2016). Zygotes segregate entire parental genomes in distinct blastomere lineages causing cleavage-stage chimerism and mixoploidy. *Genome Res*, 26(5), 567-578. doi:10.1101/gr.200527.115
- Dobson, A. T., Raja, R., Abeyta, M. J., Taylor, T., Shen, S., Haqq, C., & Pera, R. A. (2004). The unique transcriptome through day 3 of human preimplantation development. *Hum Mol Genet*, 13(14), 1461-1470. doi:10.1093/hmg/ddh157
- Elowe, S., Dulla, K., Uldschmid, A., Li, X., Dou, Z., & Nigg, E. A. (2010). Uncoupling of the spindle-checkpoint and chromosome-congression functions of BubR1. *J Cell Sci*, 123(Pt 1), 84-94. doi:10.1242/jcs.056507
- Elowe, S., Hummer, S., Uldschmid, A., Li, X., & Nigg, E. A. (2007). Tension-sensitive Plk1 phosphorylation on BubR1 regulates the stability of kinetochore microtubule interactions. *Genes Dev*, 21(17), 2205-2219. doi:10.1101/gad.436007
- Fang, G. (2002). Checkpoint protein BubR1 acts synergistically with Mad2 to inhibit anaphase-promoting complex. *Mol Biol Cell*, 13(3), 755-766. doi:10.1091/mbc.01-09-0437
- Fogarty, N. M. E., McCarthy, A., Snijders, K. E., Powell, B. E., Kubikova, N., Blakeley, P., . . . Niakan, K. K. (2017). Genome editing reveals a role for OCT4 in human embryogenesis. *Nature*, 550(7674), 67-73. doi:10.1038/nature24033
- Foygel, K., Choi, B., Jun, S., Leong, D. E., Lee, A., Wong, C. C., . . . Yao, M. W. (2008). A novel and critical role for Oct4 as a regulator of the maternal-embryonic transition. *PLoS One*, 3(12), e4109. doi:10.1371/journal.pone.0004109
- Ganem, N. J., Godinho, S. A., & Pellman, D. (2009). A mechanism linking extra centrosomes to chromosomal instability. *Nature*, 460(7252), 278-282. doi:10.1038/nature08136
- Gascoigne, K. E., & Taylor, S. S. (2008). Cancer cells display profound intra- and interline variation following prolonged exposure to antimetabolic drugs. *Cancer Cell*, 14(2), 111-122. doi:10.1016/j.ccr.2008.07.002
- Hassold, T., Chen, N., Funkhouser, J., Jooss, T., Manuel, B., Matsuura, J., . . . Jacobs, P. A. (1980). A cytogenetic study of 1000 spontaneous abortions. *Ann Hum Genet*, 44(2), 151-178. doi:10.1111/j.1469-1809.1980.tb00955.x
- Homer, H., Gui, L., & Carroll, J. (2009). A spindle assembly checkpoint protein functions in prophase I arrest and prometaphase progression. *Science*, 326(5955), 991-994. doi:10.1126/science.1175326
- Hornak, M., Kubicek, D., Broz, P., Hulinska, P., Hanzalova, K., Griffin, D., . . . Rubes, J. (2016). Aneuploidy Detection and mtDNA Quantification in Bovine Embryos with Different Cleavage Onset Using a Next-Generation Sequencing-Based Protocol. *Cytogenet Genome Res*, 150(1), 60-67. doi:10.1159/000452923
- Huang, H., Hittle, J., Zappacosta, F., Annan, R. S., Hershko, A., & Yen, T. J. (2008). Phosphorylation sites in BubR1 that regulate kinetochore attachment, tension, and mitotic exit. *J Cell Biol*, 183(4), 667-680. doi:10.1083/jcb.200805163
- Huang, H., & Yen, T. J. (2009). BubR1 is an effector of multiple mitotic kinases that specifies kinetochore: microtubule attachments and checkpoint. *Cell Cycle*, 8(8), 1164-1167. doi:10.4161/cc.8.8.8151
- Huang, J., Yan, L., Fan, W., Zhao, N., Zhang, Y., Tang, F., . . . Qiao, J. (2014). Validation of multiple annealing and looping-based amplification cycle sequencing for 24-chromosome aneuploidy screening of cleavage-stage embryos. *Fertil Steril*, 102(6), 1685-1691. doi:10.1016/j.fertnstert.2014.08.015
- Huang, Y., Jiang, L., Yi, Q., Lv, L., Wang, Z., Zhao, X., . . . Shi, Q. (2012). Lagging chromosomes entrapped in micronuclei are not 'lost' by cells. *Cell Res*, 22(5), 932-935. doi:10.1038/cr.2012.26
- Johnson, D. S., Gemelos, G., Baner, J., Ryan, A., Cinnioglu, C., Banjevic, M., . . . Rabinowitz, M. (2010). Preclinical validation of a microarray method for full molecular karyotyping of blastomeres in a 24-h protocol. *Hum Reprod*, 25(4), 1066-1075. doi:10.1093/humrep/dep452

- Kettenbach, A. N., Schweppe, D. K., Faherty, B. K., Pechenick, D., Pletnev, A. A., & Gerber, S. A. (2011). Quantitative phosphoproteomics identifies substrates and functional modules of Aurora and Polo-like kinase activities in mitotic cells. *Sci Signal*, 4(179), rs5. doi:10.1126/scisignal.2001497
- Kiessling, A. A., Bletsa, R., Desmarais, B., Mara, C., Kallianidis, K., & Loutradis, D. (2009). Evidence that human blastomere cleavage is under unique cell cycle control. *J Assist Reprod Genet*, 26(4), 187-195. doi:10.1007/s10815-009-9306-x
- Kiessling, A. A., Bletsa, R., Desmarais, B., Mara, C., Kallianidis, K., & Loutradis, D. (2010). Genome-wide microarray evidence that 8-cell human blastomeres over-express cell cycle drivers and under-express checkpoints. *J Assist Reprod Genet*, 27(6), 265-276. doi:10.1007/s10815-010-9407-6
- Krueger, F., Andrews, S. R., & Osborne, C. S. (2011). Large scale loss of data in low-diversity illumina sequencing libraries can be recovered by deferred cluster calling. *PLoS One*, 6(1), e16607. doi:10.1371/journal.pone.0016607
- Lampson, M. A., & Kapoor, T. M. (2005). The human mitotic checkpoint protein BubR1 regulates chromosome-spindle attachments. *Nat Cell Biol*, 7(1), 93-98. doi:10.1038/ncb1208
- Lee, J., Lee, U., Kim, B., & Yoon, J. (2013). A computational method for detecting copy number variations using scale-space filtering. *BMC Bioinformatics*, 14, 57. doi:10.1186/1471-2105-14-57
- Li, D., Morley, G., Whitaker, M., & Huang, J. Y. (2010). Recruitment of Cdc20 to the kinetochore requires BubR1 but not Mad2 in *Drosophila melanogaster*. *Mol Cell Biol*, 30(13), 3384-3395. doi:10.1128/MCB.00258-10
- Lightfoot, D. A., Kouznetsova, A., Mahdy, E., Wilbertz, J., & Hoog, C. (2006). The fate of mosaic aneuploid embryos during mouse development. *Dev Biol*, 289(2), 384-394. doi:10.1016/j.ydbio.2005.11.001
- Macaulay, I. C., Haerty, W., Kumar, P., Li, Y. I., Hu, T. X., Teng, M. J., . . . Voet, T. (2015). G&T-seq: parallel sequencing of single-cell genomes and transcriptomes. *Nat Methods*, 12(6), 519-522. doi:10.1038/nmeth.3370
- Madin, S. H., & Darby, N. B., Jr. (1958). Established kidney cell lines of normal adult bovine and ovine origin. *Proc Soc Exp Biol Med*, 98(3), 574-576. doi:10.3181/00379727-98-24111
- Mantikou, E., Wong, K. M., Repping, S., & Mastenbroek, S. (2012). Molecular origin of mitotic aneuploidies in preimplantation embryos. *Biochim Biophys Acta*, 1822(12), 1921-1930. doi:10.1016/j.bbadis.2012.06.013
- Mayer, W., Smith, A., Fundele, R., & Haaf, T. (2000). Spatial separation of parental genomes in preimplantation mouse embryos. *J Cell Biol*, 148(4), 629-634. doi:10.1083/jcb.148.4.629
- McCoy, R. C. (2017). Mosaicism in Preimplantation Human Embryos: When Chromosomal Abnormalities Are the Norm. *Trends Genet*, 33(7), 448-463. doi:10.1016/j.tig.2017.04.001
- McCoy, R. C., Demko, Z., Ryan, A., Banjevic, M., Hill, M., Sigurjonsson, S., . . . Petrov, D. A. (2015). Common variants spanning PLK4 are associated with mitotic-origin aneuploidy in human embryos. *Science*, 348(6231), 235-238. doi:10.1126/science.aaa3337
- McCoy, R. C., Demko, Z. P., Ryan, A., Banjevic, M., Hill, M., Sigurjonsson, S., . . . Petrov, D. A. (2015). Evidence of Selection against Complex Mitotic-Origin Aneuploidy during Preimplantation Development. *PLoS Genet*, 11(10), e1005601. doi:10.1371/journal.pgen.1005601
- McCoy, R. C., Newnham, L. J., Ottolini, C. S., Hoffmann, E. R., Chatzimeletiou, K., Cornejo, O. E., . . . Handyside, A. H. (2018). Tripolar chromosome segregation drives the association between maternal genotype at variants spanning PLK4 and aneuploidy in human preimplantation embryos. *Hum Mol Genet*. doi:10.1093/hmg/ddy147
- Menasha, J., Levy, B., Hirschhorn, K., & Kardon, N. B. (2005). Incidence and spectrum of chromosome abnormalities in spontaneous abortions: new insights from a 12-year study. *Genet Med*, 7(4), 251-263. doi:10.1097/01.gim.0000160075.96707.04
- Meraldi, P., & Sorger, P. K. (2005). A dual role for Bub1 in the spindle checkpoint and chromosome congression. *EMBO J*, 24(8), 1621-1633. doi:10.1038/sj.emboj.7600641
- Middelkamp, S., van Tol, H. T. A., Spierings, D. C. J., Boymans, S., Guryev, V., Roelen, B. A. J., . . . Kuijk, E. W. (2020). Sperm DNA damage causes genomic instability in early embryonic development. *Sci Adv*, 6(16), eaaz7602. doi:10.1126/sciadv.aaz7602

- Miller, J. F., Williamson, E., Glue, J., Gordon, Y. B., Grudzinskas, J. G., & Sykes, A. (1980). Fetal loss after implantation. A prospective study. *Lancet*, 2(8194), 554-556. doi:10.1016/s0140-6736(80)91991-1
- Miyazawa, K. (2011). Encountering unpredicted off-target effects of pharmacological inhibitors. *J Biochem*, 150(1), 1-3. doi:10.1093/jb/mvr053
- Perez-Mongiovi, D., Malmanche, N., Bousbaa, H., & Sunkel, C. (2005). Maternal expression of the checkpoint protein BubR1 is required for synchrony of syncytial nuclear divisions and polar body arrest in *Drosophila melanogaster*. *Development*, 132(20), 4509-4520. doi:10.1242/dev.02028
- Plante, L., Plante, C., Shepherd, D. L., & King, W. A. (1994). Cleavage and 3H-uridine incorporation in bovine embryos of high in vitro developmental potential. *Mol Reprod Dev*, 39(4), 375-383. doi:10.1002/mrd.1080390405
- Ramirez-Gonzalez, R. H., Bonnal, R., Caccamo, M., & Maclean, D. (2012). Bio-samtools: Ruby bindings for SAMtools, a library for accessing BAM files containing high-throughput sequence alignments. *Source Code Biol Med*, 7(1), 6. doi:10.1186/1751-0473-7-6
- Reichmann, J., Nijmeijer, B., Hossain, M. J., Eguren, M., Schneider, I., Politi, A. Z., . . . Ellenberg, J. (2018). Dual-spindle formation in zygotes keeps parental genomes apart in early mammalian embryos. *Science*, 361(6398), 189-193. doi:10.1126/science.aar7462
- Rocafort, E., Enciso, M., Leza, A., Sarasa, J., & Aizpurua, J. (2018). Euploid embryos selected by an automated time-lapse system have superior SET outcomes than selected solely by conventional morphology assessment. *J Assist Reprod Genet*, 35(9), 1573-1583. doi:10.1007/s10815-018-1265-7
- Salavert Torres J, B. E. I., Dominguez AT, Hernandez Garcia V, Medina Castello I, Tarraga Gimenez J., & J, D. B. (2012). Using GPUs for the exact alignment of short-read genetic sequences by means of the Burrows-Wheeler transform. *IEEE/ACM Trans Comput Biol Bioinform*, 9, 1245-1256.
- Santamaria, A., Wang, B., Elowe, S., Malik, R., Zhang, F., Bauer, M., . . . Nigg, E. A. (2011). The Plk1-dependent phosphoproteome of the early mitotic spindle. *Mol Cell Proteomics*, 10(1), M110 004457. doi:10.1074/mcp.M110.004457
- Schaeffer, A. J., Chung, J., Heretis, K., Wong, A., Ledbetter, D. H., & Lese Martin, C. (2004). Comparative genomic hybridization-array analysis enhances the detection of aneuploidies and submicroscopic imbalances in spontaneous miscarriages. *Am J Hum Genet*, 74(6), 1168-1174. doi:10.1086/421250
- Schindelin, J., Arganda-Carreras, I., Frise, E., Kaynig, V., Longair, M., Pietzsch, T., . . . Cardona, A. (2012). Fiji: an open-source platform for biological-image analysis. *Nat Methods*, 9(7), 676-682. doi:10.1038/nmeth.2019
- Schmid, M., Steinlein, C., Tian, Q., Hanlon Newell, A. E., Gessler, M., Olson, S. B., . . . Fedorov, L. M. (2014). Mosaic variegated aneuploidy in mouse BubR1 deficient embryos and pregnancy loss in human. *Chromosome Res*, 22(3), 375-392. doi:10.1007/s10577-014-9432-x
- Schneider, I., & Ellenberg, J. (2019). Mysteries in embryonic development: How can errors arise so frequently at the beginning of mammalian life? *PLoS Biol*, 17(3), e3000173. doi:10.1371/journal.pbio.3000173
- Schvartzman, J. M., Sotillo, R., & Benezra, R. (2010). Mitotic chromosomal instability and cancer: mouse modelling of the human disease. *Nat Rev Cancer*, 10(2), 102-115. doi:10.1038/nrc2781
- Singla, S., Iwamoto-Stohl, L. K., Zhu, M., & Zernicka-Goetz, M. (2020). Autophagy-mediated apoptosis eliminates aneuploid cells in a mouse model of chromosome mosaicism. *Nat Commun*, 11(1), 2958. doi:10.1038/s41467-020-16796-3
- Soto, M., Raaijmakers, J. A., & Medema, R. H. (2019). Consequences of Genomic Diversification Induced by Segregation Errors. *Trends Genet*. doi:10.1016/j.tig.2019.01.003
- Sugimura, S., Akai, T., Hashiyada, Y., Somfai, T., Inaba, Y., Hirayama, M., . . . Imai, K. (2012). Promising system for selecting healthy in vitro-fertilized embryos in cattle. *PLoS One*, 7(5), e36627. doi:10.1371/journal.pone.0036627
- Suijkerbuijk, S. J., Vleugel, M., Teixeira, A., & Kops, G. J. (2012). Integration of kinase and phosphatase activities by BUBR1 ensures formation of stable kinetochore-microtubule attachments. *Dev Cell*, 23(4), 745-755. doi:10.1016/j.devcel.2012.09.005

- Suzuki, K., Sako, K., Akiyama, K., Isoda, M., Senoo, C., Nakajo, N., & Sagata, N. (2015). Identification of non-Ser/Thr-Pro consensus motifs for Cdk1 and their roles in mitotic regulation of C2H2 zinc finger proteins and Ect2. *Sci Rep*, 5, 7929. doi:10.1038/srep07929
- Taylor, T. H., Gitlin, S. A., Patrick, J. L., Crain, J. L., Wilson, J. M., & Griffin, D. K. (2014). The origin, mechanisms, incidence and clinical consequences of chromosomal mosaicism in humans. *Hum Reprod Update*, 20(4), 571-581. doi:10.1093/humupd/dmu016
- Touati, S. A., Buffin, E., Cladiere, D., Hached, K., Rachez, C., van Deursen, J. M., & Wassmann, K. (2015). Mouse oocytes depend on BubR1 for proper chromosome segregation but not for prophase I arrest. *Nat Commun*, 6, 6946. doi:10.1038/ncomms7946
- Treff, N. R., Krisher, R. L., Tao, X., Gamsey, H., Bohrer, C., Silva, E., . . . Duncan, F. E. (2016). Next Generation Sequencing-Based Comprehensive Chromosome Screening in Mouse Polar Bodies, Oocytes, and Embryos. *Biol Reprod*, 94(4), 76. doi:10.1095/biolreprod.115.135483
- Tsuiko, O., Catteuw, M., Zamani Esteki, M., Destouni, A., Bogado Pascottini, O., Besenfelder, U., . . . Robert Vermeesch, J. (2017). Genome stability of bovine in vivo-conceived cleavage-stage embryos is higher compared to in vitro-produced embryos. *Hum Reprod*, 32(11), 2348-2357. doi:10.1093/humrep/dex286
- Tsuiko, O., Jatsenko, T., Parameswaran Grace, L. K., Kurg, A., Vermeesch, J. R., Lanner, F., . . . Salumets, A. (2019). A speculative outlook on embryonic aneuploidy: Can molecular pathways be involved? *Dev Biol*, 447(1), 3-13. doi:10.1016/j.ydbio.2018.01.014
- Vanneste, E., Voet, T., Le Caignec, C., Ampe, M., Konings, P., Melotte, C., . . . Vermeesch, J. R. (2009). Chromosome instability is common in human cleavage-stage embryos. *Nat Med*, 15(5), 577-583. doi:10.1038/nm.1924
- Vazquez-Diez, C., Paim, L. M. G., & FitzHarris, G. (2019a). Cell-Size-Independent Spindle Checkpoint Failure Underlies Chromosome Segregation Error in Mouse Embryos. *Curr Biol*. doi:10.1016/j.cub.2018.12.042
- Vazquez-Diez, C., Paim, L. M. G., & FitzHarris, G. (2019b). Cell-Size-Independent Spindle Checkpoint Failure Underlies Chromosome Segregation Error in Mouse Embryos. *Curr Biol*, 29(5), 865-873 e863. doi:10.1016/j.cub.2018.12.042
- Vazquez-Diez, C., Yamagata, K., Trivedi, S., Haverfield, J., & FitzHarris, G. (2016). Micronucleus formation causes perpetual unilateral chromosome inheritance in mouse embryos. *Proc Natl Acad Sci U S A*, 113(3), 626-631. doi:10.1073/pnas.1517628112
- Vera-Rodriguez, M., Chavez, S. L., Rubio, C., Reijo Pera, R. A., & Simon, C. (2015). Prediction model for aneuploidy in early human embryo development revealed by single-cell analysis. *Nat Commun*, 6, 7601. doi:10.1038/ncomms8601
- Vitak, S. A., Torkenczy, K. A., Rosenkrantz, J. L., Fields, A. J., Christiansen, L., Wong, M. H., . . . Adey, A. (2017). Sequencing thousands of single-cell genomes with combinatorial indexing. *Nat Methods*, 14(3), 302-308. doi:10.1038/nmeth.4154
- Webster, A., & Schuh, M. (2017). Mechanisms of Aneuploidy in Human Eggs. *Trends Cell Biol*, 27(1), 55-68. doi:10.1016/j.tcb.2016.09.002
- Wei, Y., Multi, S., Yang, C. R., Ma, J., Zhang, Q. H., Wang, Z. B., . . . Sun, Q. Y. (2011). Spindle assembly checkpoint regulates mitotic cell cycle progression during preimplantation embryo development. *PLoS One*, 6(6), e21557. doi:10.1371/journal.pone.0021557
- Wilcox, A. J., Weinberg, C. R., & Baird, D. D. (1995). Timing of sexual intercourse in relation to ovulation. Effects on the probability of conception, survival of the pregnancy, and sex of the baby. *N Engl J Med*, 333(23), 1517-1521. doi:10.1056/NEJM199512073332301
- Wong, C. C., Loewke, K. E., Bossert, N. L., Behr, B., De Jonge, C. J., Baer, T. M., & Reijo Pera, R. A. (2010). Non-invasive imaging of human embryos before embryonic genome activation predicts development to the blastocyst stage. *Nat Biotechnol*, 28(10), 1115-1121. doi:10.1038/nbt.1686
- Yao, T., Suzuki, R., Furuta, N., Suzuki, Y., Kabe, K., Tokoro, M., . . . Sugimura, S. (2018). Live-cell imaging of nuclear-chromosomal dynamics in bovine in vitro fertilised embryos. *Sci Rep*, 8(1), 7460. doi:10.1038/s41598-018-25698-w
- Zhang, C. Z., Spektor, A., Cornils, H., Francis, J. M., Jackson, E. K., Liu, S., . . . Pellman, D. (2015). Chromothripsis from DNA damage in micronuclei. *Nature*, 522(7555), 179-184. doi:10.1038/nature14493

- Zhang, G., Mendez, B. L., Sedgwick, G. G., & Nilsson, J. (2016). Two functionally distinct kinetochore pools of BubR1 ensure accurate chromosome segregation. *Nat Commun*, 7, 12256. doi:10.1038/ncomms12256
- Zhou, B., Ho, S. S., Zhang, X., Pattni, R., Haraksingh, R. R., & Urban, A. E. (2018). Whole-genome sequencing analysis of CNV using low-coverage and paired-end strategies is efficient and outperforms array-based CNV analysis. *J Med Genet*, 55(11), 735-743. doi:10.1136/jmedgenet-2018-105272
- Zimin, A. V., Delcher, A. L., Florea, L., Kelley, D. R., Schatz, M. C., Puiu, D., . . . Salzberg, S. L. (2009). A whole-genome assembly of the domestic cow, *Bos taurus*. *Genome Biol*, 10(4), R42. doi:10.1186/gb-2009-10-4-r42
- Zinaman, M. J., Clegg, E. D., Brown, C. C., O'Connor, J., & Selevan, S. G. (1996). Estimates of human fertility and pregnancy loss. *Fertil Steril*, 65(3), 503-509. doi: 10.1016/j.fertnstert.2019.08.096